UNIVERSITÀ DEGLI STUDI DI PADOVA

Dipartimento di Fisica e Astronomia "Galileo Galilei"

Corso di Laurea Magistrale in Fisica

Tesi di Laurea

Beyond Mean Field Effects in Quasi-1D Dipolar Bosonic Quantum Gases: Roton Mode and Supersolid Behaviour

Relatore

Prof. Francesco Ancilotto

Contro relatore

Prof. Pier Luigi Silvestrelli

Laureando

Santo Maria Roccuzzo

Anno Accademico 2017/2018

Contents

Introduction

A BEC (acronym for Bose-Einstein Condensate) is a degenerate state of matter that forms in extreme conditions, at a temperature close to the absolute zero, and in extremely dilute samples (with density of order 10^{14} or 10^{15} $atoms/cm^3$, while ordinary matter has a typical density of 10^{22} $atoms/cm^3$). The main feature of a BEC is that a macroscopic number of particles condensates into the state of lower energy available, as consequence of quantum statistical effects.
The existance of the BEC phase was proposed by S. Bose (1924) and A. Einstein (1925), but its occurrence in a real system was recognized only much later, with the discovery of superfluidity in liquid helium [1, 2], and the intuition by F. London (1938) that this new phase of matter could be a manifestation of Bose-Einstein condensation [3].
The physics of superfluid helium and its connections with Bose-Einstein condensation was then extensively studied in the subsequent years from both a theoretical (we mention the pioneering works of L. Tisza (1938) [4] and L. Landau (1941)[5], with the developed of the two-fluid model, and N. Bogoliubov (1947)[6], who instead developed the microscopic theory of weakly interacting bosons) and experimental point of view. For long time, the study of superfluidity and Bose-Einstein condensation was limited to the study of the properties of liquid helium, as helium is the only element that remains liquid as the temperature gets closer to the absolute zero, while all other elements becomes solids. In order to extend the study of Bose Einstein condensation and superfluidity also to other elements, it became clear the necessity of using very dilute samples, in order to prevent solidification. Moreover, most of the theories in Bose-Einstein condensation requires the hypothesis of weak interactions, that cannot be satisfied in a liquid sample. For these reasons, during the 1970s and 1980s, great experimental efforts were devoted to the realization of the BEC phase in weakly interacting, ultradilute gases. Several techniques based on the use of laser beams were developed to trap and cool gases of alkali atoms, until finally, in 1995, the first BECs were obtained in alkali gases by the experimental groups led by J. Coleman and C. Wieman [7] at Boulder and W. Ketterle [8] at MIT.
The realization of BECs in atomic trapped gases introduced several novel features due to the fact that, in these systems, the coupling of the atoms with the trapping electric and magnetic fields allows to *tune* the strength and even the sign of the interatomic interaction (using techniques based on the knowledge of the so-called *Feshbach resonances* [9] of the atomic species). Moreover, while most theories developed before 1995 considered only homogeneous, infinite systems, this new kind of BECs are inhomogeneous and

strongly confined.
From a theoretical point of view, the fact that BECs of trapped gases are ultracold and extremely dilute simplifies the general many body problem, as in these conditions only s-wave scattering between atoms usually takes place, and so the actual, complex interatomic potential can be replaced by a simpler pseudo-potential, usually of the form of a hard-sphere repulsion, and described by a single parameter, the s-wave scattering length. However, this simple, short-range interaction sufficies to explain the phenomenon of superfluidity. This led, over the last years, to the research of different possible types of interactions, that can eventually lead to the formation of new and exotic phases of matter.
In this research, the dipole-dipole interaction attracted great attention for different reasons. First, there are several experimental techniques to efficiently trap and cool atoms (or molecules) possessing a strong dipole moment. This led, for example, to the experimental realization of BECs made of ^{52}Cr in 2006 [10] or, more recently, of the more magnetic lanthanides ^{164}Dy and ^{166}Er[11, 12]. Moreover, the dipole-dipole interaction, being anisotropic and long-ranged, is the only possible interaction between ultracold (neutral) atoms that cannot be simplified with an effective short-range pseudo-potential. This leads to unique observable properties of dipolar BECs.
One peculiarity of dipolar BECs is their geometry-dependent stability. In fact, due to the partially attractive nature of the dipole-dipole interaction, to obtain a stable dipolar BEC one needs to confine the atoms in reduced dimensions, in particular in quasi-2D strongly oblate traps, or in quasi-1D strongly prolate traps, always orthogonally to the polarization direction. In these conditions, the attractive part of the dipole-dipole interaction can be balanced by the repulsive nature of short-range interactions, leading finally to a stable BEC. Recent experiments [13] studied the stability diagram of ^{52}Cr as function of the scattering length and trap geometry, and found that in an extremely anisotropic trap, if the BEC is very tightly confined along the polarization direction, it is possible even to tune the scattering length to zero, and so to realize a purely dipolar BEC. If instead the dipoles are not confined enough, if the scattering length is reduced below a certain threshold, the attractive part of the dipolar interaction prevails, and the BEC phase is destroyed (in the sense that no BEC can be revealed anymore) by the interaction induced collapse.
Similar experiments [14, 15] has been performed also using a BEC of ^{164}Dy, whose magnetic moment is higher then that of ^{52}Cr. Due to its strongly magnetic nature, even in very anisotropic traps, the attractive part of dipole-dipole interaction plays a fundamental role. The experiments showed in fact a surprising feature. Starting with a stable dipolar BEC of ^{164}Dy in a disk-shaped trap and reducing its scattering length below a certain threshold does not result in the destruction of the condensate, but rather to the formation of an ordered array of denser atomic clusters. Other experiments [16] shows that these clusters are actually self-bound quantum droplets. Several theoretical studies [17, 18] have demonstrated that the collapse of the dipolar BEC is arrested by quantum fluctuations, through a mechanism that will be exstensively discussed in this thesis.
The transition from the stable BEC to an ordered array of self-bound droplets is trig-

gered by a "roton-instability", that is a particular kind of excitation that forms a local minimum at finite momentum. The energy of the minimum is called "roton-gap", and is usually reduced if the mechanism that leads to the formation of the roton minimum is enhanced. When the roton-gap becomes null, a modulation of the density with the roton wavelength costs no energy, and thus the ground state of the system can host a periodic structure.
The ordered state that is formed is often called in literature "crystal cluster", indicating a structure that possesses the typical symmetry for discrete translations of a solid, but in which the points of the Bravais lattice are occupied by clusters containing also several thousands of atoms. However, it must always be clear that we are dealing with extremely dilute systems: even if the droplets have a density which is around one order of magnitude higher then that of the initial BEC, it is still several orders of magnitude lower then that of ordinary matter.
In this crystal cluster, it is possible that a fraction of the atoms is detached from the droplets, and so can form a "halo" of dilute superfluid in which the system is immersed. For this reason, this system is ideal for the reaserch of the exotic phase of *supersolidity*, that is a phase that shares features typical of solids (and in particular the symmetry for *discrete* translations) and superfluids (such as the frictionless transport of matter and global phase coherence).
The present thesis is inspired by a recent experimental work [19], in which it has been shown that a dipolar BEC of ^{166}Er in a strongly prolate ("cygar-shaped") trap can show the features described above. In particular, the experiment shows that, reducing the scattering length of the initially stable BEC leads to the formation of a "roton population", signalled by the presence, in the measured momentum distribution, of two symmetric peaks at finite momenta.
We thus explore, through numerical simulations based on a Density Functional approach, the equilibrium structure and elementary excitations of a dipolar BEC confined in a quasi-1D "ring" geometry, in order to study the conditions for the formation of a crystal cluster of the type described above, and to understand if this state shows supersolid behaviour. We simulate a ring geometry by confining the dipoles inside a "tube", orthogonal to the polarization direction, and enforcing periodic boundary conditions to "match" the two extrema of the tube. We choose this geometry because in the ring it is possible to accomodate a perfectly periodical structure, and moreover it is accessible to experiments. Thus, this model is ideal for the possible detection of a supersolid state.
This thesis is structured as follows.
In chapter 1, we review the main theoretical results that allow to describe a dipolar BEC. The fundamental instruments for the description of the ground state and elementary excitations are presented.
In chapter 2, we present the numerical tools used to explore both the ground state and the elementary excitations. Moreover, we show some test of the codes used against results described in the recent literature on the subject.
In chapter 3, we present a preliminar variational study, in which a simple model allows to understand the fundamental, qualitative features of the system under study.

In chapters 4, 5 and 6 we show the results of the numerical simulations, that allows to characterize a phase transition from a homogeneous superfluid to a crystal cluster, that shows supersolid behaviour.

Chapter 1

Theory of dipolar BECs

In this chapter we review the main properties and features of dipolar BECs. We present the definition and main properties of dipole-dipole interaction, and briefly describe the typical atomic or molecular systems in which it can be found. Then, we give a brief review of Density Functional Theory, and show how it can be applied to study the mean-field ground state and elementary excitations. Finally, we show how mean-field theory must be modified in order to partially take into account the effects of quantum fluctuations, that will be introduced using an approach known as "Local Density Approximation".

1.1 Dipole-Dipole interaction

Let us consider the typical case in which the dipoles are aligned by an external field, and fix the z-axis of a reference frame along this direction. Then the dipole-dipole interaction for two identical dipoles reads

$$V_{dd}(\mathbf{r}-\mathbf{r}') = \frac{C_{dd}}{4\pi}\frac{1-3cos^2\theta}{|\mathbf{r}-\mathbf{r}'|^3} \tag{1.1}$$

where $C_{dd} = \mu_0\mu^2$ for two magnetic dipoles of magnetic moment μ (and μ_0 is the permeability of the vacuum) and $C_{dd} = d^2/\epsilon_0$ for two identical electric dipoles with electric dipole moment d (and ϵ_0 is the vacuum permittivity). Moreover, $\mathbf{r}-\mathbf{r}'$ is the relative position of the dipoles and θ is the angle between this and the polarization direction.
The relative strength of electric and magnetic dipolar interaction between polar atoms (or molecules) can be estimated using a simple argument [20, 21]. The typical size of an atomic or molecular electric dipole moment is of order $d \simeq ea_0$, where e is the electron charge and a_0 is the Bohr radius (the order of magnitude is that of one Debye). Instead, a typical atomic magnetic moment is of order of the Bohr magneton μ_B. The relative strength can be thus estimated as

$$\frac{\mu_0\mu^2}{d^2/\epsilon_0} = \epsilon_0\mu_0\frac{\mu_B^2}{e^2a_0^2} \tag{1.2}$$

Using the definitions $a_0 = \frac{\hbar}{m_e c \alpha}$, $\mu_B = \frac{e\hbar}{2m_e c}$ and $\epsilon_0 \mu_0 = c^{-2}$, where m_e is the electron mass, c is the speed of light, and α is the fine structure constant, one finds

$$\frac{\mu_0 \mu^2}{\frac{d^2}{\epsilon_0}} \simeq \alpha^{-2} \simeq 10^{-4} \tag{1.3}$$

Thus, at the atomic and molecular scale, the interaction between electric dipoles is typically much stronger than that between magnetic dipoles.
A very usefull quantity that allows to quantify the strength of dipolar interaction is the *dipolar length* a_{dd}, defined as

$$a_{dd} = \frac{C_{dd} m}{12\pi\hbar^2} \tag{1.4}$$

The dipolar length allows to give a more quantitative comparison between the typical strength of electric and magnetic dipolar interaction. Consider in fact the data reported in table 1.1 and taken from [20, 21]. We notice again that the dipolar length for electric dipoles is much higher than that of magnetic dipoles. Moreover, an electric dipole is usually found in a heteronuclear molecule, while a strong permanent magnetic dipole moment can be found in some atomic species. An electric dipole can also be induced in an atom by an external magnetic field, but, at the moment of writing, no electric dipolar effect has been observed in atomic BECs.
From the data of table 1.1, it is clear that the ideal candidates for the study of dipolar effects are heteronuclear molecules. However, experimental difficulties have, until now, prevented the achievement of the quantum degeneracy in polar molecules, while, as stated in the introduction, dipolar BECs have been realized with magnetic atoms. For this reason, the rest of the present thesis will be dedicated just to the magnetic case. Even if for magnetic species the interaction is much weaker then the electric case, this interaction still affects crucially the observable properties of the BEC.

Species	Dipole moment	a_{dd}
^{52}Cr	$6\mu_B$	$15a_0$
^{164}Dy	$9.9\mu_B$	$130a_0$
^{166}Er	$7\mu_B$	$65.5a_0$
KRb	$0.6D$	$2 \times 10^3 a_0$
HCN	$3D$	$2.4 \times 10^4 a_0$

Table 1.1: Magnetic and electric dipole moments for different atomic and molecular species

Consider now the form of the dipole-dipole interaction defined in 1.1. We notice that the interaction is long-ranged in 3D, decaying at large distances as r^{-3}, while the typical van der Waals interaction between the atoms of a gas decays as r^{-6}. Moreover, the interaction is anisotropic, having the symmetry of the second Legendre polynomial $P_2(cos\theta)$. It is thus null at the angle $\theta_m = arccos(1/\sqrt{3})$ (the so called "magic angle"), it is positive and thus repulsive for $0 < \theta < \theta_m$ and attractive otherwise. This implies that dipoles sitting "side-by-side" tend to repel each other, while dipoles in "head-to-tail" configuration attract each other.

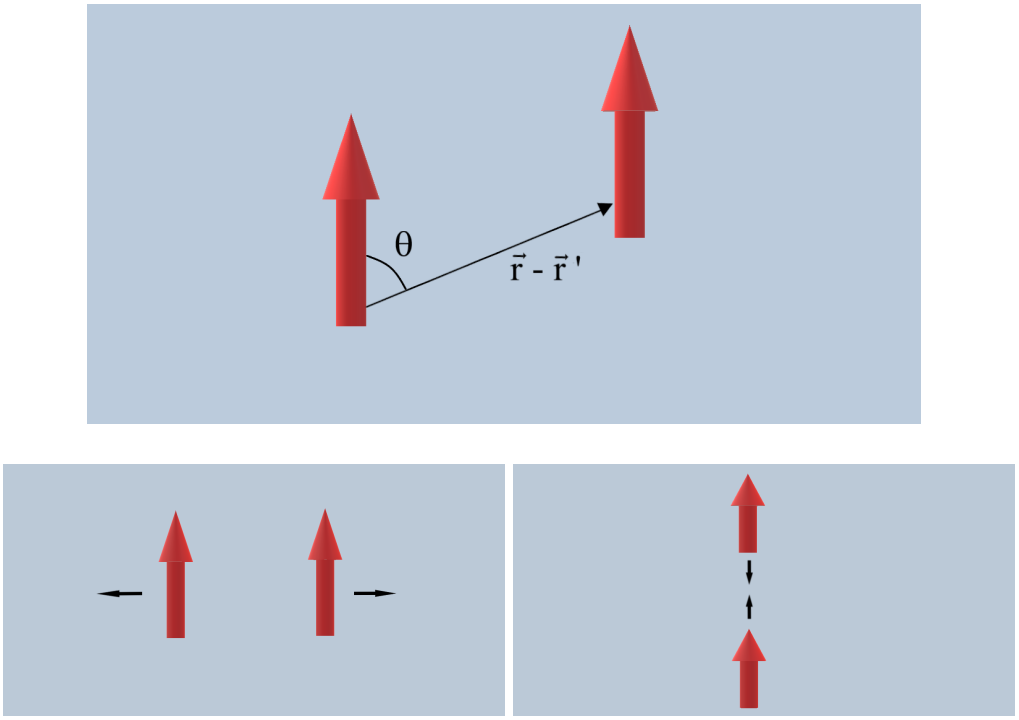

Figure 1.1: Anisotropy of the dipole-dipole interaction

This anisotropy implies that in a 3D dipolar gas, the dipole-dipole interaction is partially attractive. The gas thus tend to elongate along the polarization direction, in order to reduce its energy, and, in absence of any stabilization mechanism, to collapse. The collapse of a dipolar BEC has been experimentally studied in [22], in which it is shown that dipolar interaction crucially affects the post-collapse dinamics. In BECs with only short range interactions, the possibility of tuning the scattering length even to a negative value allows to change the sign of the interparticle interaction, that can thus be modified from repulsive to attractive. This modification of the sign of the interparticle interaction leads to an isotropic collapse of the BEC, followed by a sudden, still isotropic, expansion that finally destroys the condensate [23, 24]. This phenomenon is often called "Bose-Nova", for its qualitative similarity to the contraction and sudden expansion of a dying star that results in the famous, catastrophic astronomic events of "Supernovae". Instead, the post-collapse dynamics of a dipolar BEC is influenced by the dipolar interaction, as the expansion is not isotropic, but follows the d-wave symmetry of the dipolar potential.
To stabilize an ultracold gas of dipolar atoms, it is thus necessary to provide some stabilization mechanism. As mentioned previously, a crucial factor is the confinement geometry of the BEC, that allows to partially hide the attractive part of the interaction if the BEC is confined in the polarization direction. However, even if the confinement is very strong, some additional stabilization mechanism must be at work in order to obtain

a stable BEC. This additional mechanism is provided by short-range interactions, whose strength is quantified by the s-wave scattering length a. This can be tuned in experiment, and a sufficiently high, positive value of a, together with the geometrical confinement, can allow the achievement of a stable BEC in presence of dipolar interaction. It is thus crucial to quantify the relative strength of dipolar and contact interaction. For this reason, we can define the *dipolar parameter* ϵ_{dd} as

$$\epsilon_{dd} = \frac{a_{dd}}{a} \tag{1.5}$$

If $\epsilon_{dd} < 1$, the particles tend, in average, to repel each other, and so the dipolar collapse is prevented. Instead, if $\epsilon_{dd} > 1$, the attractive part of the dipolar interaction tends to prevail, and so the system is expected to be unstable against collapse.
We are now ready to present the theoretical framework in which we study dipolar BECs. We start with a brief review of Density Functional Theory, and then explain how to use the theory for the study of a dipolar BEC.

1.2 Density Functional Theory

The calculations presented in this thesis are all based on a Density Functional approach, adapted to the description of a BEC of dipolar atoms.
In a real system of ultracold atoms in which the BEC phase is realized, only a finite fraction of atoms actually occupy the ground state, even at $T = 0$. In fact, a pure BEC, in which all the atoms are in the ground state, can be obtained in principle only for a non-interacting system, as the interparticle interactions force a finite fraction of atoms into the first excited states. This phenomenon is known as *quantum depletion*, and can be limited only in very dilute samples. Nevertheless, we suppose to be in a condition in which quantum depletion can be neglected, so that, at $T = 0$, all the atoms are in the BEC phase.
In Density Functional Theory, instead of solving the Schrödinger equation of the N particle system in order to determine the ground state wave function, we determine the *ground state density* of the system using a variational principle.
The theory is based on the two famous theorems by Hohenberg and Kohn (1964) [25]. The first theorem can be formulated as follows [26]:

Theorem 1. *Let $\Psi_{gs}(\mathbf{r}_1, \mathbf{r}_2, ..., \mathbf{r}_N)$ be the many-body wave function of the ground state of N interacting particles, and define the ground state density of the system as*

$$n_{gs}(\mathbf{r}) = \int d\mathbf{r}_2 ... d\mathbf{r}_N \Psi_{gs}(\mathbf{r}, \mathbf{r}_2, ..., \mathbf{r}_N) \tag{1.6}$$

Then, there is a one-to-one correspondence between the external potential V_{ext} acting on the system and the ground state density n_{gs}.

We omit the proof here, as it can be found in the cited references, and limit ourselves to discuss its implications.

The theorem implies that once we fix the external potential, the ground state density is determined *uniquely*. A corollary of the first theorem is that

Corollary 1.1. *We can define a universal functional of the density*

$$F[n_{gs}] = \langle \Psi_{gs} | (T + U) | \Psi_{gs} \rangle \tag{1.7}$$

where T and U are respectively the kinetic and the interparticle interaction energy, so that the total ground-state energy is given by

$$E[n_{gs}] = F[n_{gs}] + \int d\mathbf{r} V_{ext}(\mathbf{r}) n_{gs}(\mathbf{r}) \tag{1.8}$$

The corollary implies that, once the ground state density is fixed, so is the total energy.
The second theorem of Hohenberg and Kohn allows to find the ground state density from a variational principle. It states that

Theorem 2. *For any trial density n, we have $E[n] \geq E[n_{gs}]$, and the equality holds if and only if $n = n_{gs}$.*

So, the ground state energy of the system is in one-to-one correspondence with the ground state density, which in turn can be determined through a variational approach, minimizing the energy functional itself. However, to have reliable results, the main issue is to find a good model for $F[n]$. For what concern the expression of the kinetic energy as functional of the density, the typical approach is to use the Kohn-Sham [27] approximation, that is an independent particle approximation in which the actual kinetic energy is approximated by the kinetic energy of a *fictitious* non-interacting system, but with *the same density* as the real one. We thus introudce the so called Kohn-Sham orbitals ϕ_i, requiring them to satisfy

$$n(\mathbf{r}) = \sum_{i=1}^{N} |\phi_i(\mathbf{r})|^2 \tag{1.9}$$

and suppose that the wave function of the system can be approximated as

$$\Psi(\mathbf{r}_1, \mathbf{r}_2, ..., \mathbf{r}_N) = \phi_1(\mathbf{r}_1).....\phi_N(\mathbf{r}_N) \tag{1.10}$$

Notice that this expression can be used only for a system of bosons, as Ψ is unchanged under the exchange of two particles. Instead, for describing a system of fermions, one needs to use a Slater determinant of Kohn-Sham orbitals in order to ensure the correct symmetry of Ψ. However, in our case, in which all the particles occupy the ground state

ϕ_0, the Kohn-Sham expression of the kinetic energy is given by

$$\begin{aligned} T_0[n] &= \int d\mathbf{r_1}...d\mathbf{r}_N \Psi^*(\mathbf{r}_1, \mathbf{r}_2, ..., \mathbf{r}_N) \left(\sum_{i=1}^{N} -\frac{\hbar^2 \nabla_i^2}{2m} \right) \Psi(\mathbf{r}_1, \mathbf{r}_2, ..., \mathbf{r}_N) \\ &= \sum_{i=1}^{N} \phi_i^*(\mathbf{r}) \left(-\frac{\hbar^2 \nabla_i^2}{2m} \right) \phi_i(\mathbf{r}) \\ &= N \int d\mathbf{r} \phi_0^* \left(-\frac{\hbar^2 \nabla^2}{2m} \right) \phi_0(\mathbf{r}) \end{aligned} \tag{1.11}$$

For what concern the interparticle interaction energy U, a first, typical approach is that of approximating it with a mean field expression. In particular, we can use the Kohn-Sham form of Ψ to evaluate this energy term as

$$\begin{aligned} U_H &= \int d\mathbf{r}_1...d\mathbf{r}_N \phi_0^*(\mathbf{r}_1)...\phi_0^*(\mathbf{r}_N) \left(\frac{1}{2} \sum_{i \neq j} V(\mathbf{r}_i - \mathbf{r}_j) \right) \phi_0(\mathbf{r}_1)...\phi_0(\mathbf{r}_N) \\ &= \frac{1}{2} N(N-1) \int d\mathbf{r} d\mathbf{r}' |\phi_0(\mathbf{r})|^2 V(\mathbf{r} - \mathbf{r}') |\phi_0(\mathbf{r}')|^2 \end{aligned} \tag{1.12}$$

Notice that this is nothing but the classical Hartree [28] approximation of the energy of N interacting particles.
If we sum the Kohn-Sham expressions of T_0 and U_H, we obtain an approximate expression for the ground-state energy of the system

$$\begin{aligned} E[\phi_0] =& N \int d\mathbf{r} \phi_0^*(\mathbf{r}) \left(-\frac{\hbar^2 \nabla^2}{2m} + V_{ext}(\mathbf{r}) \right) \phi_0(\mathbf{r}) \\ &+ \frac{1}{2} N(N-1) \int d\mathbf{r} d\mathbf{r}' |\phi_0(\mathbf{r})|^2 V(\mathbf{r} - \mathbf{r}') |\phi_0(\mathbf{r}')|^2 \end{aligned} \tag{1.13}$$

We now define the *condensate wave-function* ϕ as

$$\phi = \sqrt{N} \phi_0 \tag{1.14}$$

whose squared modulus equals the local density $n(\mathbf{r})$, and rewrite the energy 1.13, in the limit of large N, as

$$\begin{aligned} E[\phi] =& \int d\mathbf{r} \phi^*(\mathbf{r}) \left(-\frac{\hbar^2 \nabla^2}{2m} + V_{ext}(\mathbf{r}) \right) \phi(\mathbf{r}) \\ &+ \frac{1}{2} \int d\mathbf{r} d\mathbf{r}' |\phi(\mathbf{r})|^2 V(\mathbf{r} - \mathbf{r}') |\phi(\mathbf{r}')|^2 \end{aligned} \tag{1.15}$$

Notice that, if ϕ_0 is normalized to 1, then ϕ is normalized to the total number of particles N.

We insert these approximations into the energy functional 1.8 as

$$\begin{aligned} E[n] &= T_0 + U_H + \int d\mathbf{r} V_{ext}(\mathbf{r}) n(\mathbf{r}) + (T - T_0 + U - U_H) \\ &= T_0 + U_H + \int d\mathbf{r} V_{ext}(\mathbf{r}) n(\mathbf{r}) + E_{corr} \end{aligned} \tag{1.16}$$

where we have defined the correlation energy E_{corr} as the term that takes into account the corrections to the mean-field approximation. Good models clearly require the evaluation of at least some approximation of the correlation energy E_{corr}. A typical approach is the Local Density Approximation [29], in which one approximate

$$E_{corr} = \int d\mathbf{r} \epsilon_{corr}(\mathbf{r}) \tag{1.17}$$

where ϵ_{corr} is the correlation energy per unit volume of the homogeneous system, and can usually be calculated, at least perturbatively, using the methods of quantum field theory.
We are now ready to apply the machinery of Density Functional Theory to the study of a dipolar BEC.

1.3 Mean Field Theory of dipolar BECs

1.3.1 Ground state

Following the results of the previous section, we consider a system of interacting bosons at zero temperature and introduce the *condensate wave function* ϕ, defined in such a way that its square modulus equals the local density n

$$|\phi(\mathbf{r})|^2 = n(\mathbf{r}) \tag{1.18}$$

We then define a mean-field energy functional for the condensate as

$$E[\phi] = \int d\mathbf{r} \phi^*(\mathbf{r}) \left(-\frac{\hbar^2}{2m} \nabla^2 + V_{ext}(\mathbf{r}) \right) \phi(\mathbf{r}) + \frac{1}{2} \int d\mathbf{r} d\mathbf{r}' |\phi(\mathbf{r})|^2 V(\mathbf{r} - \mathbf{r}') |\phi(\mathbf{r}')|^2 \tag{1.19}$$

where V is the two-body interaction potential. So, we determine the mean field equation for the description of the condensate wave function by functional minimization of the energy. Moreover, we fix the total number of particles, so that the variational approach corresponds to the solution of the functional equation

$$\frac{\delta}{\delta \phi^*} \left[E - \mu \left(N - \int d\mathbf{r} n(\mathbf{r}) \right) \right] = 0 \tag{1.20}$$

This way, we obtain a mean field equation for ϕ as

$$\mu \phi(\mathbf{r}) = \left(-\frac{\hbar^2}{2m} \nabla^2 + V_{ext}(\mathbf{r}) + V_{mf}(\mathbf{r}) \right) \phi(\mathbf{r}) \tag{1.21}$$

where the mean field potential V_{mf} is defined as

$$V_{mf}(\mathbf{r}) = \int d\mathbf{r}' V(\mathbf{r}-\mathbf{r}')|\phi(\mathbf{r}')|^2 \tag{1.22}$$

The time dependent version of 1.21 can be defined as

$$i\hbar\frac{\partial}{\partial t}\Phi(\mathbf{r},t) = \left(-\frac{\hbar^2}{2m}\nabla^2 + V_{ext}(\mathbf{r}) + V_{mf}(\mathbf{r})\right)\Phi(\mathbf{r},t) \tag{1.23}$$

so that a trial solution of the form

$$\Phi(\mathbf{r},t) = \phi(\mathbf{r})e^{-i\frac{\mu}{\hbar}t} \tag{1.24}$$

implies that ϕ is the solution of 1.21. The Lagrange multiplier μ is the chemical potential, that fixes the total number of particles.
A key point is to find a good model for the two-body potential. The typical interaction potential between neutral, non-dipolar atoms is a van der Waals potential, which is strongly repulsive at short distances, then becomes attractive at "intermediate" distances, and finally decays as r^{-6} at long distances. The exact shape can also be quite complicated, and it is calculated via semi-empirical models or *ab-initio*. However, in the case of a very dilute, ultracold gas, we have important simplifications to this problem.
Usually, the interatomic potential possesses two-particles bound states, that form when the distance between the two atoms is of order of a few Angstroms and the temperature is low enough. Because of the fact that a BEC is formed at a temperature close to the absolute zero, the ground state of any system (with the only exception of ^4He) at that temperature would be a solid. Thus, the BEC is a metastable phase, that is created under conditions of extreme diluteness. The typical density is 10^{14} or $10^{15} atoms/cm^3$. Moreover, even in this conditions, there are three-body recombination mechanisms that gradually leads to the formation of bound states and destroy the condensate.
Recalling the fundamental results of scattering theory [30], we have that, for a central potential decaying like r^{-n}, the phase shifts $\delta_l(k)$, for $k \to 0$, behave as k^{2l+1} for $n > 3$, and as k^{n-2} otherwise. This means that, at low temperatures and in absence of dipolar interaction, only s-wave scattering ($l = 0$) is important, and the entire scattering process is described by a single parameter, the s-wave scattering length a. This allows to substitute the actual, complicated, but short-ranged, two-body potential, with a *pseudo-potential* that reproduces the same scattering properties, namely the same scattering length. In the case of hard-sphere interaction, if a is the radius of the sphere, as shown in [31], a good pseudo-potential is given by

$$V_{pseudo}(r) = \frac{4\pi\hbar^2 a}{m}\delta(r)\frac{\partial}{\partial r}r = g\delta(r)\frac{\partial}{\partial r}r \tag{1.25}$$

Crucially, this result is still valid for interactions that, in three dimensions, decay *faster* then r^{-3} at long distances. Inserting 1.25 in 1.21, we obtain the Gross-Pitajevskii equation [32]

$$\mu\phi(\mathbf{r}) = \left(-\frac{\hbar^2}{2m}\nabla^2 + V_{ext}(\mathbf{r}) + g|\phi(\mathbf{r})|^2\right)\phi(\mathbf{r}) \tag{1.26}$$

which has been very successfull in explaining the experimentally observed properties of non dipolar BECs [32].
The case of dipolar interaction is clearly peculiar because, as it decays as r^{-3} at large distances and being anisotropic, it cannot be replaced by the isotropic pseudo-potential 1.25. This happens because all the partial waves contributes to the scattering amplitude. However, it would clearly be usefull to generalize 1.26 to describe also the dipolar case. In [33, 34], it has been shown that a pseudo-potential of the form

$$V_{pseudo}(\mathbf{r}) = g\delta(r)\frac{\partial}{\partial r}r + V_{dd}(\mathbf{r}) \tag{1.27}$$

successfully reproduces, at the level of the Born approximation, the scattering amplitude given by a general short range potential plus the dipole-dipole potential 1.1. Even if this result is only perturbative, it can be used to generalize 1.26, inserting 1.27 into 1.23, obtaining a non-linear, non local Schrödinger equation

$$i\hbar\frac{\partial}{\partial t}\Phi(\mathbf{r},t) = \left(-\frac{\hbar^2}{2m}\nabla^2 + V_{ext}(\mathbf{r}) + g|\Phi(\mathbf{r},t)|^2 + \int d\mathbf{r}' V_{dd}(\mathbf{r}-\mathbf{r}')|\Phi(\mathbf{r}',t)|^2\right)\Phi(\mathbf{r},t) \tag{1.28}$$

and its time independent version

$$\mu\phi(\mathbf{r}) = \left(-\frac{\hbar^2}{2m}\nabla^2 + V_{ext}(\mathbf{r}) + g|\phi(\mathbf{r})|^2 + \int d\mathbf{r}' V_{dd}(\mathbf{r}-\mathbf{r}')|\phi(\mathbf{r}')|^2\right)\phi(\mathbf{r}) \tag{1.29}$$

This Non-Local Gross-Pitajevskii Equation (NLGPE) will be used in this work as a starting point for the description of the mean field ground state of a dipolar BEC.

1.3.2 Elementary excitations

To describe the elementary excitations of a dipolar BEC, we can use a standard Bogoliubov-de Gennes approach and search for a solution of 1.28 of the form

$$\Phi(\mathbf{r},t) = e^{-i\frac{\mu}{\hbar}t}[\phi(\mathbf{r}) + \delta\phi(\mathbf{r},t)] \tag{1.30}$$

where ϕ is the solution of 1.29, while the fluctuation $\delta\phi$ is expanded as

$$\delta\phi(\mathbf{r},t) = u(\mathbf{r})e^{-i\omega t} - v^*(\mathbf{r})e^{i\omega t} \tag{1.31}$$

Keeping only terms linear in the quasi-particle amplitudes u and v, we obtain the Bogoliubov-de Gennes (BdG) equations

$$\begin{aligned}
\hbar\omega u(\mathbf{r}) = &\left[-\frac{\hbar^2}{2m}\nabla^2 - \mu + V_{ext}(\mathbf{r}) + \int d\mathbf{r}' V(\mathbf{r}-\mathbf{r}')|\phi(\mathbf{r}')|^2\right]u(\mathbf{r}) \\
&+\phi(\mathbf{r})\int d\mathbf{r}' V(\mathbf{r}-\mathbf{r}')[\phi^*(\mathbf{r}')u(\mathbf{r}') - \phi(\mathbf{r}')v(\mathbf{r}')] \\
-\hbar\omega v(\mathbf{r}) = &\left[-\frac{\hbar^2}{2m}\nabla^2 - \mu + V_{ext}(\mathbf{r}) + \int d\mathbf{r}' V(\mathbf{r}-\mathbf{r}')|\phi(\mathbf{r}')|^2\right]v(\mathbf{r}) \\
&+\phi^*(\mathbf{r})\int d\mathbf{r}' V(\mathbf{r}-\mathbf{r})[\phi(\mathbf{r}')v(\mathbf{r}') - \phi^*(\mathbf{r}')u(\mathbf{r}')]
\end{aligned} \tag{1.32}$$

This is a set of coupled integro-differential equations, very difficult to solve even numerically. In general, it is convenient to cast it in a matrix form

$$\begin{pmatrix} H_0 + \hat{X} & -\hat{X}^\dagger \\ \hat{X} & -H_0 + \hat{X}^\dagger \end{pmatrix} \begin{pmatrix} u \\ v \end{pmatrix} = \hbar\omega \begin{pmatrix} u \\ v \end{pmatrix} \tag{1.33}$$

with

$$H_0 = -\frac{\hbar^2}{2m}\nabla^2 - \mu + V_{ext}(\mathbf{r}) + \int d\mathbf{r}' V(\mathbf{r} - \mathbf{r}')|\phi(\mathbf{r}')|^2 \tag{1.34}$$

and the operator $\hat{X}$ acts on a general function f as

$$\hat{X} f(\mathbf{r}) = \phi(\mathbf{r}) \int d\mathbf{r}' V(\mathbf{r} - \mathbf{r}')\phi^*(\mathbf{r}')f(\mathbf{r}') \tag{1.35}$$

A particular case is that of a 3D homogeneous system (for which one needs clearly to put $V_{ext} = 0$). Even if this system is not realistic, it serves as a prototype of more realistic conditions. In [35], the authors shows that, for this case, the BdG equations 1.32 become algebraic in Fourier space, and can be solved for the excitation spectrum, as well as for the amplitudes u and v. A complete calculation is given in the appendix, while here we just say that the excitation spectrum is given by

$$\hbar\omega_{\mathbf{k}} = \sqrt{\frac{\hbar^2 k^2}{2m}\left[\frac{\hbar^2 k^2}{2m} + 2n_0\tilde{V}_{\mathbf{k}}\right]} \tag{1.36}$$

where $\tilde{V}_{\mathbf{k}}$ is the Fourier transform of the pseudo-potential 1.27, defined as

$$\tilde{V}_{\mathbf{k}} = \int d\mathbf{r} V(\mathbf{r}) e^{-i\mathbf{k}\cdot\mathbf{r}} \tag{1.37}$$

The complete calculation is again reported in the appendix, while here we just report that the final result is

$$\tilde{V}_{\mathbf{k}} = g\left[1 + \epsilon_{dd}(3cos^2\alpha - 1)\right] \tag{1.38}$$

where α is the angle between $\mathbf{k}$ and the polarization direction, the *dipolar parameter* ϵ_{dd} is defined as

$$\epsilon_{dd} = \frac{\mu_0\mu^2}{3g} = \frac{a_{dd}}{a} \tag{1.39}$$

and a_{dd} is again the *dipolar length*, that quantify the strength of the dipolar interaction

$$a_{dd} = \frac{\mu_0\mu^2 m}{12\pi\hbar^2} \tag{1.40}$$

For clearness, we rewrite the excitation spectrum explicitly as

$$\hbar\omega_{\mathbf{k}} = \sqrt{\frac{\hbar^2 k^2}{2m}\left[\frac{\hbar^2 k^2}{2m} + g\left[1 + \epsilon_{dd}(3cos^2\alpha - 1)\right]\right]} \tag{1.41}$$

Some important properties come out from the form of 1.41. It is clear that the dispersion relation is anisotropic, as a consequence of the anisotropy of the dipole-dipole interaction. Moreover, for $\epsilon_{dd} < 1$ all the modes are stable, meaning that all the excitation energies are real and positive. Instead, for $\epsilon_{dd} > 1$ the argument under the square root of 1.41 can become negative in the $k \to 0$ limit, meaning that phonon modes of long wavelength can acquire imaginary frequencies, expecially for a propagation direction orthogonal to the polarization axis. Thus, a stable 3D uniform dipolar BEC can in principle be created, provided that $a_{dd} < a$. Instead, for $a_{dd} > a$, a 3D uniform dipolar BEC is destabilized by long wavelength modes propagating orthogonally to the polarization axis.
For a confined, inhomogeneous dipolar BEC, this is not necessarily true anymore. In fact, by confining the dipoles for example in a very oblate trap, perpendicular to the polarization direction, it is possible to create a quasi-2D dipolar BEC, that remains stable even for $\epsilon_{dd} > 1$. In fact, in a quasi-2D geometry orthogonal to the polarization direction, the dipoles mainly repel each other, and so the attractive part of the interaction, responsible for the instability, can be "hidden". The stability of a dipolar BEC as function of the scattering length and the trapping geometry has been explored experimentally in [13] with a BEC made of ^{52}Cr in a cylindrically symmetric oblate trap, finding results which are in good agreement with mean-field estimates based on the solution of 1.29[20].
However, the validity of a mean-field description of a dipolar BEC has been challanged by the experimental results reported in [14]. In the cited work, the authors study the stability of a BEC of ^{164}Dy, which is the atom with the strongest permanent magnetic dipole moment in the periodic table, equal to $\mu \simeq 9.98\mu_B$. They prepared a stable BEC in the quasi-2D geometry of the type discussed, with $\epsilon_{dd} \simeq 1$, and then performed a rapid quench in the scattering length to a certain low value (as compared with the value of a_{dd} of ^{164}Dy) using the knowledge of the Feshbach resonances of Dysprosium. This way, they observed an initial collapse of the BEC, followed not by the destruction of the condensate, but rather by the formation of clusters of atoms, with a density which is much higher than that of an ordinary BEC, although still several orders of magnitude lower than that of ordinary matter. Moreover, in subsequent experiments [36], the authors managed to isolate single clusters by magnetic levitation, and found that these systems are *self-bound*. Thus, these experiments shows that the collapse of a dipolar BEC can lead to the formation of structures that can be defined as *quantum droplets*, that is self-bound, relatively dense clusters of atoms.
An accurate theoretical study of droplet formation has proved to be a difficult task. As reported in [17], simulations based on 1.29 leads to the prediction of the collapse of the initial BEC once the scattering length is reduced below a certain value. This implies that the formation of self-bound quantum droplets in a dipolar BEC is a *beyond-mean-field* phenomenon.
To gain an insight on droplet formation, we now present the beyond-mean-field theory for dipolar BECs, that allows to partially take into account the effects of quantum fluctuations.

1.4 Beyond mean field: the Lee-Huang-Yang correction

The beyond-mean-field mechanism that leads to the formation of self-bound quantum droplets in dipolar BECs has been first proposed in [17], and it is based on a similar mechanism as that proposed in [37] to explain droplet formation in Bose-Bose mixtures. The mechanism is based on the fact that the first beyond-mean-field correction to the ground state energy of a system of N bosons interacting through the pseudopotential 1.27 at T colse to zero is positive and increases with the density. Thus, as the initial condensate collapses, its energy is reduced, but at the same time, the beyond-mean-field correction to the ground state energy increases, until an equilibrium condition is reached in which a further collapse is no more energetically convenient. So, quantum droplets are stabilized by the interplay between a mean-field attraction, that is triggered when the attractive part of the dipole-dipole interaction prevails on the repulsive nature of short range interactions, and beyond-mean-field repulsion, that gets stronger and stronger as the density increases, until an equilibrium condition is reached.
The theoretical background is that of the Lee-Huang-Yang (LHY) correction to the ground state energy of a system of "hard spheres" bosons, first proposed in [31]. A detailed calculation of the correction is given in the appendices, in which it is also shown how to generalize the calculation to include general interactions. In particular, we can show that, in the case of a homogeneous system of dipolar bosons, the ground state energy of the system up to first order quantum corrections is given by

$$\frac{E_0}{V} = \frac{1}{2}gn^2\left[1 + \frac{128}{15\sqrt{\pi}}\sqrt{na^3}F(\epsilon_{dd})\right] \tag{1.42}$$

with

$$F(\epsilon_{dd}) = \frac{1}{2}\int_0^\pi d\theta sin\theta[1 + \epsilon_{dd}(3cos^2\theta - 1)]^{\frac{5}{2}} \tag{1.43}$$

To calculate the effect of this energy shift in the non-homogeneous case, following [17] we use here an approach based on Local Density Approximation, that is consider a LHY contribution to the total energy given by

$$E_{LHY} = \frac{2}{5}\gamma(\epsilon_{dd})\int d\mathbf{r}n(\mathbf{r})^{\frac{5}{2}} \tag{1.44}$$

with

$$\gamma(\epsilon_{dd}) = \frac{32}{3\sqrt{\pi}}ga^{\frac{3}{2}}F(\epsilon_{dd}) \tag{1.45}$$

Adding this to the energy functional 1.19 and minimizing with respect to ϕ^*, we finally obtain an extended NLGPE, which incorporates beyond-mean-field effects

$$\begin{aligned}\mu\phi(\mathbf{r}) =& \Big(-\frac{\hbar^2}{2m}\nabla^2 + V_{ext}(\mathbf{r}) + g|\phi(\mathbf{r})|^2 + \\ &\int d\mathbf{r}'|\phi(\mathbf{r}')|^2 V_{dd}(\mathbf{r}-\mathbf{r}') + \gamma(\epsilon_{dd})|\phi(\mathbf{r})|^3\Big)\phi(\mathbf{r})\end{aligned} \tag{1.46}$$

As shown in [17], simulations based on the solution of this equation leads to the description of droplet formation, in good agreement with the experimental results reported in [14].
The introduction of the LHY correction in the NLGPE makes necessary to recalculate also the BdG equations, in order to take into account the effects of quantum fluctuations on the excitation spectrum. Using the same approach as in the previous section, we arrive at an extended matrix form of 1.33, with the replacements

$$\begin{aligned} H_0 &\to H_0 + \gamma(\epsilon_{dd})|\phi|^3 \\ \hat{X} &\to \hat{X} + \frac{3}{2}\gamma(\epsilon_{dd})|\phi|^3 \end{aligned} \tag{1.47}$$

The extended version of NLGPE 1.46 and of the BdG equations 1.47 will be solved numerically in this thesis in order to study the ground state and elementary excitations of a dipolar BEC. However, before presenting the numerical methods used, we show that a *roton instability*, namely an elementary excitation that forms a local minimum in the excitation spectrum at a finite momentum, is closely related to the formation of quantum droplets in a dipolar BEC. Moreover, we show that this two related phenomena (roton instability and quantum droplets) are at the basis of a phase transition from an ordinary BEC to a possible exotic phase of matter known as *supersolid*, which is a hypothesized phase of matter that shares features of solids and superfluids, and that, at the moment of writing, has not yet been detected unambiguously.

1.5 Roton mode and supersolid behaviour

A "roton" is an elementary excitation of a homogeneous BEC that forms a local minimum at a finite momentum. The existence of this kind of excitation was first proposed by L. Landau [5] in his theory of superfluid helium, and initially related to the possible formation of vortices. The predictions of Landau were experimentally tested [38], and the excitation spectrum of liquid helium was measured in 1961. Its qualitative behaviour is reported in figure 1.2.

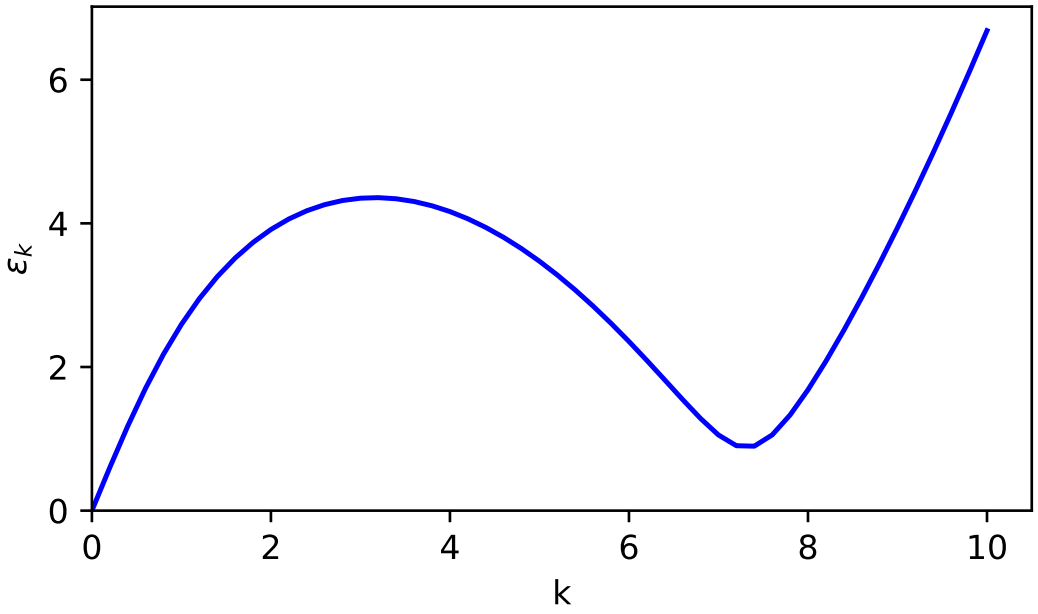

Figure 1.2: Qualitative reproduction of the measured excitation spectrum of superfluid helium. Arbitrary units are used

From the form of 1.36, we can see that, a necessary condition for the excitation spectrum to develop a minimum at finite momentum, is that the Fourier transform of the interaction potential is negative in some range of the interaction parameters. So, by tuning the interaction parameters in a BEC, a roton minimum can be formed in the excitation spectrum, and if one enhance the mechanism that leads to the formation of the roton minimum, the energy of the roton, called *roton gap*, can be reduced, until it becomes null. In this condition, the *excitation of the roton mode costs no energy*. Thus, the ground state of the system can show a modulation of the density, with a wavelength determined by the critical value of the momentum at which the roton gap disappears.
So, the "softening" of the roton mode, that is the reduction of the roton gap, can cause a phase transition from a homogeneous superfluid to a periodic structure, whose symmetry for discrete translations resemble that of a crystal. In this "crystal" structure, what we find [39, 40] is an ordered array of clusters of atoms, each one occupying one site of a periodic lattice. Moreover, in this ordered structure, a partial superfluid flow between different clusters is possible.
At this point, it is important to make a fundamental remark. Very often in literature one encounters the term "crystal" to describe the ordered lattice of atomic clusters described above. However, one must always keep in mind that we are dealing with extremely dilute systems, with densities which are orders of magnitude lower than that of ordinary matter. Moreover, this ordered structures have the peculiar feature that a partial superfluid flow is possible between different lattice sites, so that global phase coherence is possible

throughout the entire lattice. This mechanism can be at the base of the formation of a possible phase of matter known as *supersolid*.
A supersolid can be defined as a system in which the symmetry of crystals for discrete translations coexists with the global phase coherence of a superfluid [40]. The existance of this phase and its unambiguous detection has been a matter of debate for long time. In fact, a seminal paper of Penrose and Onsager (1956) [41] showed that the localization of particles of a crystalline phase and the delocalization of particles in a superfluid phase are incompatible. However, this work is not a demonstration that no supersolid phase can exist at all, and in fact the possibility of a density modulation in a superfluid, with the discrete symmetry of crystals, was pointed out soon after by Gross (1957)[42]. Successive works of Yang (1962) [43] and Leggett (1970) [44] suggested that in solid helium the "hopping" of atoms between adjacent lattice sites can in fact be significant, and the superfluid response of solid helium could be measured.
The coexistance of a crystal and a superfluid phase was later invoked to explain the observation of non-classical rotational inertia (NCRI) in solid helium [45]. However, the same authors of [45] later challenged their own experimental results[46].
Nonetheless, in recent years, a great theoretical and experimental effort has been dedicated to the search for a supersolid phase in other systems, in particular in the field of ultracold atoms. Several works, as for example [47, 48], show that good candidates for the reaserch of a supersolid phase are systems of soft-core bosons, that are systems of bosons interacting through a pseduo-potential of the form

$$V(r) = V_0\Theta(r - R_c) \tag{1.48}$$

where R_c is the range of the interaction, V_0 is its *finite* strength, and Θ is the Heaviside step function. In a BEC of soft-core bosons, the softening of the roton mode leads to the formation of a periodic structure in which denser atomic clusters are immersed in a dilute superfluid background.
To characterize a supersolid phase, we can define some *computable* and *measurable* quantity associated to supersolid behaviour. One of such quantities, that represents the fundamental hallmark of supersolid behaviour, is the Non-Classical Intertia (NCI).
The NCI is due to the fact that the superfluid fraction of the system does not share the translational or rotational motion of the crystal structure, as it flows without friction through the crystal. To check, in a simulation or a theoretical calculation, if a system can show NCI, we can solve the problem of the system translating with velocity $\mathbf{v}$, starting from the energy functional 1.15 and miniziming it by requiring the system to have a fixed average momentum $\langle \mathbf{P} \rangle$, by introducing an additional constraint on the minimization

$$\frac{\delta}{\delta\phi*}\left[E - \mu\left(N - \int d\mathbf{r}|\phi(\mathbf{r})|^2\right) - \mathbf{v}\cdot\left(\langle\mathbf{P}\rangle - \int d\mathbf{r}\phi^*(\mathbf{r})(-i\hbar\nabla)\phi(\mathbf{r})\right)\right] = 0 \tag{1.49}$$

obtaining the NLGPE equation of the system in a comoving reference frame with velocity $\mathbf{v}$

$$\mu\phi = (\hat{H} + i\hbar\mathbf{v}\cdot\nabla)\phi \tag{1.50}$$

where $\hat{H}$ contains both the mean-field and beyond-mean-field terms. Then, following [49], we define the superfluid fraction, analogous to NCI, as

$$f_s = 1 - \frac{\langle \hat{\mathbf{P}} \rangle}{Nmv} \tag{1.51}$$

where $\langle \hat{\mathbf{P}} \rangle$ is the expectation value of the momentum calculated in the state ϕ solution of 1.50, N is the total number of particles and m is their mass. So, this definition corresponds to the fraction of the particles that does not participate to the translational motion of the system. If this fraction is finite, it means that if we move the "container" of the system, only a finite fraction of the atoms will be dragged by this motion. This can be considered as a signature of the presence of NCI.
Another signature of supersolidity is associated with the appearance of a gapless Goldstone mode in the excitation spectrum [47, 48] in addition to the usual phonon modes. The idea is that, according to Goldstone theorem [50], at each spontaneous breaking of a continuous symmetry corresponds the formation of a massless boson, whose dispersion relation is gapless. So, the spontaneous breaking of the continuous translational symmetry of the initial BEC leads to the appearance of the usual phonon modes, while the spontaneous breaking of global gauge symmetry responsible for superfluidity corresponds to the formation of an additional gapless mode, that manifest itself at a lower energy and can be thought of as a phonon propagating in the phase.
So, a supersolid phase can be found in a system of ultracold atoms in which the roton mode is softened and the roton gap reduced. In this thesis, we will show that such physics can be found in a BEC of dipolar atoms, but with a fundamental difference as compared with the cited references. In the cited works, in fact, the only types of interactions taken into account are *repulsive*. Instead, we will show that, in a dipolar BEC confined in the appropriate geometry, the roton mode is softened by the *attractive* part of the dipolar interaction. This has a fundamental consequence. While in a repulsive BEC, the phase transition from the homogeneous superfluid to a supersolid can be studied in a mean-field approach, in the dipolar case no stable ground state with a modulation of the density can be found in mean-field theory. As for the previously discussed case of quantum droplets, in mean-field theory the clusters of atomic dipoles are expected to collapse, while beyond-mean-field corrections allow to study the formation of a supersolid also in the dipolar case.
We now present the numerical methods used to solve the extended NLGPE 1.46 and BdG 1.33 with the addition of the beyond-mean-field term 1.47, and applied to study respectively the ground state and elementary excitations of a dipolar BEC.
We will then show that confining a dipolar BEC in a quasi-1D ring geometry and rising the dipolar parameter ϵ_{dd} defined in 1.39 over a certain threshold triggers the softening of the roton mode and the formation of a density modulation in the ground state. We will also show that this modulated structure shows the hallmarks of supersolid behaviour.

Chapter 2

Numerical methods

The simulations presented in this thesis are based on the numerical solution of the extended NLGPE 1.46 for ground state calculations, obtained by a technique known as *imaginary time evolution*, and of the BdG equations 1.33 with the addition of the beyond-mean-field term 1.47 for the calculation of the elementary excitations, obtained instead through diagonalization in Fourier space. In this chapter we explain the algorithms used and how they have been tested against results found in the literature.

2.1 Imaginary time evolution

The tecnique of imaginary time evolution of the Schrödinger equation allows for the calculation of the ground state wave function of a system.
Consider the general form of the Schrödinger equation, and let us perfom a Wick rotation to imaginary time $t \to -i\tau$, obtaining

$$-\hbar\frac{\partial}{\partial\tau}|\Psi\rangle = \hat{H}|\Psi\rangle \tag{2.1}$$

Formally, this equation can be solved as

$$|\Psi\rangle = e^{-\frac{\hat{H}}{\hbar}\tau}|\Psi_0\rangle \tag{2.2}$$

where $|\Psi_0\rangle$ is some initial state. Then, if $\{|\phi_i\rangle\}$ is an orthonormal set of eigenstates of $\hat{H}$, we can expand the initial state as

$$|\Psi_0\rangle = \sum_i c_i|\phi_i\rangle \tag{2.3}$$

where the c_i are complex coefficients. Thus, inserting 2.3 in 2.2, we obtain

$$|\Psi\rangle = \sum_i c_i e^{-\frac{E_i}{\hbar}\tau}|\phi_i\rangle \tag{2.4}$$

where we label with E_i the eigenvalues of the hamiltonian. If τ is large enough, only the ground state, namely the eigenstate with the lowest eigenvalue E_0, will contribute appreciably to 2.4, so that we find

$$|\Psi\rangle \simeq c_0 e^{-\frac{E_0}{\hbar}\tau}|\phi_0\rangle \text{ for } \tau \to \infty \tag{2.5}$$

Finally, in order to keep the final $|\Psi\rangle$ finite also in the limit $\tau \to \infty$, we introduce an energy offset equal to E_0, that is we consider an alternative version of 2.1 given by

$$-\hbar\frac{\partial}{\partial\tau}|\Psi\rangle = (\hat{H} - E_0)|\Psi\rangle \tag{2.6}$$

In the $\tau \to \infty$ limit, this equation will then give us

$$|\Psi\rangle = \lim_{\tau\to\infty} e^{-\frac{\hat{H}-E_0}{\hbar}\tau}|\Psi_0\rangle = c_0|\phi_0\rangle \tag{2.7}$$

that is, exactly the ground state.
In the present work, this technique has been used to solve the equation 1.46 iteratively. In this case, the offset is not given by the ground state energy, but by the chemical potential μ.
In the numerical simulation the solution is calculated iteratively, starting from a trial wave function $\phi_0(\mathbf{r})$, and defining

$$\phi_{n+1}(\mathbf{r}) = e^{-\frac{\hat{H}-\mu}{\hbar}\tau}\phi_n(\mathbf{r}) \simeq \left(1 - \frac{\hat{H}-\mu}{\hbar}\tau\right)\phi_n(\mathbf{r}) \tag{2.8}$$

Clearly, when starting the iterations, we do not know the correct chemical potential. For this reason, at each iteration, the best possible estimate of the chemical potential is calculated as

$$\mu_n = \frac{\langle\phi_n|\hat{H}|\phi_n\rangle}{\langle\phi_n|\phi_n\rangle} \tag{2.9}$$

Iterations then goes on until some convergence criterion is met, for example in the total energy, as explained in the following.

2.1.1 Details of the algorithm

The algorithm used is structured as follows:

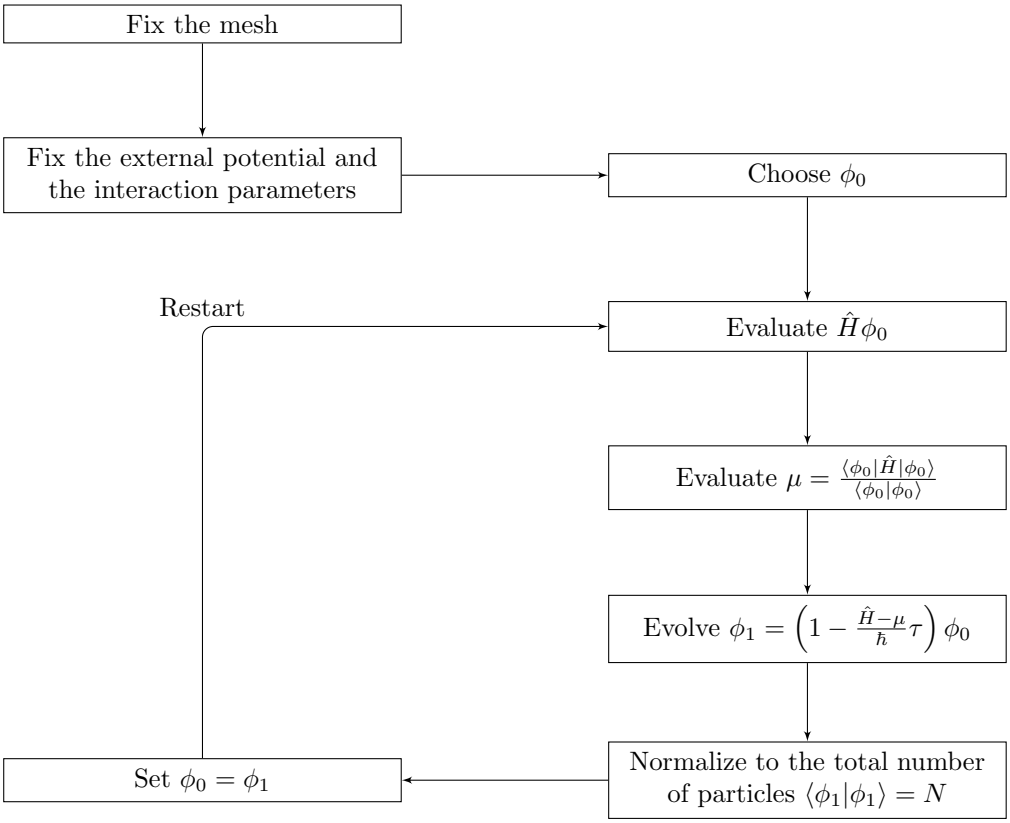

The first step is simple but fundamental. Before starting any calculation, we need to define the domain in which the calculation itself is performed. Thus, we need to choose an appropriate mesh in real space, that is find a domain of $\Re^3$ and discretize it. So, at the beginning of the simulations, a mesh in real space is created defining the points

$$\begin{aligned} x(i) &= -x_{max} + (i-1)dx \\ y(i) &= -y_{max} + (i-1)dy \\ z(i) &= -z_{max} + (i-1)dz \end{aligned} \tag{2.10}$$

where $x_{max}, y_{max}, z_{max}$ are the boundaries of the domain of simulation, i is an integer index running from 1 to the number n of mesh points along a certain direction, and the step size is given along each direction by $dx = \frac{2x_{max}}{n_x}$, $dy = \frac{2y_{max}}{n_y}$, $dz = \frac{2z_{max}}{n_z}$.
As it will be clear later, even if we will often simulate a system which is not actually periodic, it is convenient to fix periodic boundary conditions (PBC), so that a mesh in Fourier space can also be used. Usually, PBC are used to describe a system which is actually periodic. However, if we consider an isolated system, we can still fix PBC, provided that the periodic images of the system do not interact among themselves.

In this conditions, one can define, even for a non periodic system, a mesh in Fourier space as

$$\begin{aligned} k_x(i) &= -k_x^{max} + (i-1)dk_x \\ k_y(i) &= -k_y^{max} + (i-1)dk_y \\ k_z(i) &= -k_z^{max} + (i-1)dk_z \end{aligned} \tag{2.11}$$

where the maximum wave numbers are given, along each direction, by $k^{max} = h^{-1}$, where h is the step size in real space, and the step size in Fourier space is given by $dk = k_{max}/N$, where N is the number of points in real space.
The second step is to define an appropriate external potential. This is needed, in experiments, to confine the condensate and thus avoid its destruction (remember that this systems are extremely dilute). The atoms in a BEC are generally confined using an external inhomogeneous magnetic field [51]. The typical magnetic field used to trap atomic gases for realizing a BEC is called "Time-Averaged Optical Potential" (TOP) [52] and is given by the sum of a linearly varying term

$$\mathbf{B}_L = B' \left(x, y, -2z\right) \tag{2.12}$$

and a homogeneous field rotating with angular frequency ω in the x-y plane

$$\mathbf{B}_R = B_0 \left(\cos\omega t, \sin\omega t, 0\right) \tag{2.13}$$

The total magnetic field near the center of the trap has thus a magnitude given by

$$B_T = \sqrt{B_0^2 + 2B'B_0(x\cos\omega t + y\sin\omega t) + (B')^2(x^2+y^2+4z^2)} \tag{2.14}$$

We can then expand the total magnetic field around the center of the trap ($x = y = z = 0$) obtaining

$$B_T \simeq B_0 + \sqrt{2B'B_0}(x\cos\omega t + y\sin\omega t) + (B')^2(x^2+y^2+4z^2) \tag{2.15}$$

If the frequency of the rotating field is high compared to typical frequency of the atomic motion, then one can take the time average of the magnetic field over a period of one rotation, and obtain finally

$$\bar{B} \simeq B_0 + (B')^2(x^2+y^2+4z^2) \tag{2.16}$$

This approximation is valid for a frequency ω of a few kHz. This magnetic field then couples to the magnetic moment of the atoms (which is non-null also for alkali atoms, even if of the order of only $1\mu_B$ and so not sufficient to alter the observable properties of the BEC), which then feels a harmonic external potential that trap them near the center of the trap, where the potential has a minimum.
By varying the details of B_L and B_R it is possible modify the exact shape of the harmonic

potential, which is then usually given by specifying the trapping frequencies along the three spatial directions

$$V_{ext}(\mathbf{r}) = \frac{1}{2}m(\omega_x^2 x^2 + \omega_y^2 y^2 + \omega_z^2 z^2) \tag{2.17}$$

where m is the mass of the atomic species considered. Because of the fact that this kind of trapping potential is extremely common in experiment, in the simulations presented in this thesis the external potential has usually the form 2.17, for a suitable (and reasonable) choice of the trapping frequencies.
After fixing the external potential, one needs to fix the interaction paramenters. Actually, we need only to fix the scattering length a and the dipolar length a_{dd}. While the first can be tuned in experiment using the knowledge of Feshbach resonances, and so it is varied in the various simulations, the second is fixed by the permanent magnetic dipole moment of the atomic species considered, according to 1.40. For example, for ^{164}Dy we have $a_{dd} = 132a_0$, where a_0 is the Bohr radius, while for ^{166}Er we have $a_{dd} = 65.5a_0$.
Then, the choice of the inital trial wave function ϕ_0 is driven by physical intuition. In fact, starting from an initial wave function which is close to a possible solution can lead to a considerable reduction of the number of iterations needed to reach convergence. Because of the fact that ususally the external potential is harmonic, a good choice for the initial wave function is a gaussian, choosen so that its square modulus is normalized to the total number of particles N

$$\phi_0(\mathbf{r}) = \frac{\sqrt{N}}{\sqrt{2\pi}a_x a_y a_z} e^{-\frac{1}{4}\left[\left(\frac{x}{a_x}\right)^2 + \left(\frac{y}{a_y}\right)^2 + \left(\frac{z}{a_z}\right)^2\right]} \tag{2.18}$$

where the harmonic lengths are given by $a_i = \sqrt{\frac{\hbar}{m\omega_i}}$.
The next step, that is the evaluation of $\hat{H}\phi_0$, is the most difficult one. In fact, at this step, we need to calculate, for every point of the mesh,

$$\hat{H}\phi_0(\mathbf{r}) = \frac{-\hbar^2}{2m}\nabla^2\phi_0(\mathbf{r}) + V_{eff}(\mathbf{r})\phi_0(\mathbf{r}) \tag{2.19}$$

where

$$V_{eff} = V_{ext}(\mathbf{r}) + g|\phi_0(\mathbf{r})|^2 + \int d\mathbf{r}' V_{dd}(\mathbf{r} - \mathbf{r}')|\phi_0(\mathbf{r}')|^2 \tag{2.20}$$

The calculation of the action of the laplacian ∇^2 is performed using a finite-difference n-point formula, with n typically set equal to 11 in order to have a good precision. The evaluation of the effective potential is instead complicated by the presence of the integral term, which is computationally expensive in a 3D mesh. However, having choosen PBC, we can evaluate this integral in Fourier space, where, according to the convolution theorem, it is simply given by

$$\begin{aligned}\int d\mathbf{r}' V_{dd}(\mathbf{r} - \mathbf{r}')|\phi_0(\mathbf{r}')|^2 &= \int d\mathbf{r}' V_{dd}(\mathbf{r} - \mathbf{r}')n_0(\mathbf{r}') \\ &= F^{-1}(\tilde{V}_{dd}\tilde{n})\end{aligned} \tag{2.21}$$

where F^{-1} is the inverse Fourier transform. Using the FFT algorithm for the evaluation of the Fourier transform then leads to an enormous saving in computational cost.
Having computed $\hat{H}\phi_0$, the evaluation of the current estimate for the chemical potential is straightforward, and simply given by

$$\mu = \frac{\langle\phi_0|\hat{H}|\phi_0\rangle}{\langle\phi_0|\phi_0\rangle} \tag{2.22}$$

Finally, the imaginary time evolution must be performed choosing appropriately the time step τ. This can be fixed using a physical argument, noting that, if a is the step size in real space, the Heisenberg uncertainty relation fixes a zero point energy of $\frac{\hbar^2}{2ma^2}$, and thus a typical time of order $\tau \simeq \frac{2ma^2}{\hbar}$, so that a reasonable order of magnitude for the time step can fixed according to this definition. We then evolve iteratively according to 2.8 and normalize at each step the current estimate of the wave function to the total number of particles.
Iterations are stopped only when a convergence criterion is met. To fix a convergence criterion, we look at the total energy, which can be calculated, at each iteration, as

$$E_{tot} = E_{kin} + E_{ext} + E_{cont} + E_{dd} + E_{LHY} \tag{2.23}$$

with

$$\begin{aligned}
E_{kin} &= \int d\mathbf{r}\frac{\hbar^2}{2m}|\nabla n(\mathbf{r})|^2 \\
E_{ext} &= \int d\mathbf{r}V_{ext}(\mathbf{r})n(\mathbf{r}) \\
E_{cont} &= \frac{1}{2}\int d\mathbf{r}gn^2(\mathbf{r}) \\
E_{dd} &= \frac{1}{2}\int d\mathbf{r}d\mathbf{r}'V_{dd}(\mathbf{r}-\mathbf{r}')n(\mathbf{r})n(\mathbf{r}') \\
E_{LHY} &= \frac{2}{5}\gamma(\epsilon_{dd})\int d\mathbf{r}n(\mathbf{r})^{\frac{5}{2}}
\end{aligned} \tag{2.24}$$

and $n(\mathbf{r}) = |\phi(\mathbf{r})|^2$. The convergence criterion is then fixed as

$$\frac{|E_n - E_{n-1}|}{E_n} < \epsilon \tag{2.25}$$

where ϵ is of order of machine precision.

2.1.2 Code testing

The algorithm described in the previous section has been implemented in the Fortran language, and then it has been tested against results found in literature.
The first results against which the code has been tested are those presented in [53].

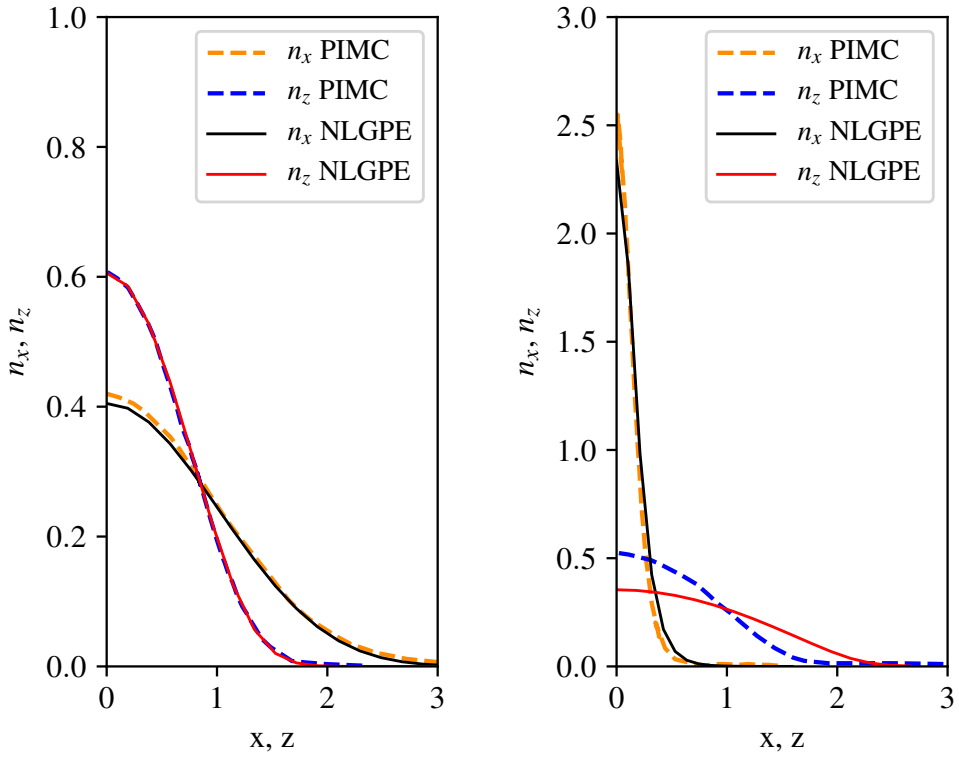

(a) Weak radial confinement

(b) Strong radial confinement

Figure 2.1: Comparison between PIMC and NLGPE 1.46 results, for $a = 70a_0$ and different radial confinements. Lengths are expressed in units of the harmonic length $a_x = \sqrt{\frac{\hbar}{m\omega_x}}$, the integrated densities are in units of a_x^{-1}

In this work, the author uses Path Integral Monte Carlo to study the ground state of a BEC made of 1024 atoms of ^{164}Dy, in a harmonic trap of frequencies $\omega_x, \omega_y, \omega_z = 2\pi(46, 44, 133)Hz$. He computes the integrated density profiles, defined as

$$\begin{aligned} n_x(x) &= \int dydzn(x, y, z) \\ n_z(z) &= \int dxdyn(x, y, z) \end{aligned} \tag{2.26}$$

for a fixed value of the scattering length $a = 70a_0$ and two different radial confinements. He finds that, for a weak radial confinement, the system is in a metastable state, from which it collapses to a droplet structure if the radial confinement is increased.
Using the codes described before and the same parameters of [53], we obtain the results shown in figure 2.1.
We can see that simulations based on NLGPE plus the LHY correction gives good re-

sults when compared with PIMC results. The only appreciable difference between the density profiles calculated with the two methods is given by the integrated density along the z-axis reported on the right panel of figure 2.1, but this difference remains inside the statistical errors that limits the accuracy of PIMC results. This means that mean field theory plus LHY correction is sufficient to describe quite accurately the systems we are interested in, without the need to use the computationally expensive Quantum Monte Carlo methods.
The second test of the codes has been performed against the results found in [18], in which the authors study the stability of self bound droplets of ^{164}Dy using the extended NLGPE 1.46. In their work, they fix the number of particles N and the value of the scattering length, compute the ground state energy, and obtain a phase diagram in which the energy of the solutions is reported as a function of N and ϵ_{dd}^{-1}. In particular, in this $N - \epsilon_{dd}^{-1}$ phase diagram, they find a stability line that separates positive and negative energy solutions, which represent, respectively, unstable and stable droplets.
We thus performed the second test against these results. In particular, we perform two "cuts" of the phase diagram: first, we perform different simulations for the fixed value of $N = 1000$ and different scattering lengths, and then we fix the scattering length to the value $a = 70a_0$ and change the number of particles. We separeted the positive from the negative energy solutions, and found that our negative energy solutions lie below the stability line, as shown in figure 2.2.

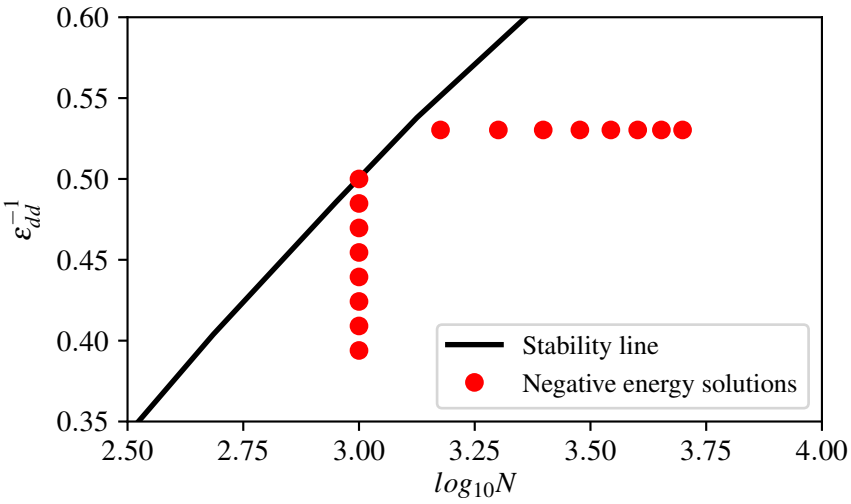

Figure 2.2: Comparison between obtained negative energy solutions of 1.46 and the phase diagram presented in [18]

Once again, our tests are in good agreement with results accepted in literature.

2.2 Bogoliubov-de Gennes equations

As stated previously, the elementary excitations of the condensate can be studied using the Bogoliubov-de Gennes equations, for example in the form 1.33 with the beyond-mean-field correction 1.47. The numerical solution of these equations is complicated by the presence of the various integral terms, that becomes computationally heavy in 3D. For this reason, it is convenient to try to exploit some symmetry of the system in order to simplify the solution.
In the case of the elementary excitations of dipolar self-bound droplets, it is possible to exploit the cylindrical symmetry of the problem around the polarization axis, as explained in [54]. In particular, in this case, each elementary excitation can be labelled by an integer number m, which corresponds to the z-projection of the angular momentum. This approach has been used in [55], but it is not applicable to the kind of systems studied in the present thesis, where, as will be explained in the following, we consider a system which is free along a direction orthogonal to the polarization direction, and tightly confined in the other two directions.
As stated in the introduction, this work focuses on the possible roton instability of a dipolar BEC in a ring geometry, that can eventually lead to the formation of a supersolid structure. We will then look for periodic structures made of stable, self-bound droplets, and so the oscillations can be expanded in the Bloch form appropriate for a periodical system, and which are labelled by a wave vector $\mathbf{k}$ and a band index n. This implies

that, when we expand the fluctuation $\delta\phi$ in the Bogoliubov-de Gennes form, we can label the quasi-particle amplitudes by $\mathbf{k}$ and n

$$\delta\phi(\mathbf{r},t) = u_{n,\mathbf{k}}(\mathbf{r})e^{-i\omega t} - v^*_{n,\mathbf{k}}(\mathbf{r})e^{i\omega t} \tag{2.27}$$

Moreover, having assumed periodic boundary conditions and defined a mesh in real space, we can take the discrete Fourier transform of the quasi-particle amplitudes, namely

$$\begin{aligned} u_{\mathbf{k}}(\mathbf{r}) &= \sum_{\mathbf{G}} u_{\mathbf{k}+\mathbf{G}} e^{i(\mathbf{k}+\mathbf{G})\cdot\mathbf{r}} \\ v_{\mathbf{k}}(\mathbf{r}) &= \sum_{\mathbf{G}} v_{\mathbf{k}+\mathbf{G}} e^{i(\mathbf{k}+\mathbf{G})\cdot\mathbf{r}} \end{aligned} \tag{2.28}$$

where the vectors $\mathbf{G}$ are the reciprocal lattice vectors associated with the mesh in real space.
The same expansion can clearly be done also for the condensate wave function

$$\phi(\mathbf{r}) = \sum_{\mathbf{G}} \phi_{\mathbf{G}} e^{i\mathbf{G}\cdot\mathbf{r}} \tag{2.29}$$

Inserting these expressions in equations 1.32, we obtain the system of linear equations

$$\begin{aligned} &\left[\frac{\hbar^2}{2M}(\mathbf{k}+\mathbf{G})^2 - \mu - \hbar\omega\right] u_{\mathbf{k}+\mathbf{G}} + \sum_{\mathbf{G}'} \tilde{U}_{\mathbf{G}-\mathbf{G}'} u_{\mathbf{k}+\mathbf{G}'} \\ &\qquad + \sum_{\mathbf{G}',\mathbf{G}''} \phi_{\mathbf{G}''-\mathbf{G}'}\phi_{\mathbf{G}-\mathbf{G}''i}\tilde{V}_{\mathbf{k}+\mathbf{G}''} u_{\mathbf{k}+\mathbf{G}'} \\ &\qquad - \sum_{\mathbf{G}',\mathbf{G}''} \phi_{\mathbf{G}''-\mathbf{G}'}\phi_{\mathbf{G}-\mathbf{G}''}\tilde{V}_{\mathbf{k}+\mathbf{G}''} v_{\mathbf{k}+\mathbf{G}'} = 0 \\ -&\left[\frac{\hbar^2}{2m}(\mathbf{k}+\mathbf{G})^2 - \mu + \hbar\omega\right] v_{\mathbf{k}+\mathbf{G}} - \sum_{\mathbf{G}'} \tilde{U}_{\mathbf{G}-\mathbf{G}'} v_{\mathbf{k}+\mathbf{G}'} \\ &\qquad - \sum_{\mathbf{G}',\mathbf{G}''} \phi_{\mathbf{G}''-\mathbf{G}'}\phi_{\mathbf{G}-\mathbf{G}''}\tilde{V}_{\mathbf{k}+\mathbf{G}''} v_{k+\mathbf{G}'} \\ &\qquad + \sum_{\mathbf{G}',\mathbf{G}''} \phi_{\mathbf{G}''-\mathbf{G}'}\phi_{\mathbf{G}-\mathbf{G}''}\tilde{V}_{\mathbf{k}+\mathbf{G}''} u_{\mathbf{k}+\mathbf{G}'} = 0 \end{aligned} \tag{2.30}$$

where the coefficients $\tilde{U}_{\mathbf{G}}$ are defined from the relation

$$\int d\mathbf{r}' V(\mathbf{r}-\mathbf{r}')|\phi(\mathbf{r}')|^2 = \sum_{\mathbf{G}} \tilde{U}_{\mathbf{G}} e^{i\mathbf{G}\cdot\mathbf{r}} \tag{2.31}$$

and the $\tilde{V}_{\mathbf{k}}$ are the Fourier components of the interparticle interaction.
The linear system 2.30 can be cast in a matrix form as

$$\begin{bmatrix} \mathbf{A} & \mathbf{B} \\ -\mathbf{B} & -\mathbf{A} \end{bmatrix} \begin{bmatrix} u_{\mathbf{k}} \\ v_{\mathbf{k}} \end{bmatrix} = \hbar\omega_{\mathbf{k}} \begin{bmatrix} u_{\mathbf{k}} \\ v_{\mathbf{k}} \end{bmatrix} \tag{2.32}$$

where the matrices A and B are defined as

$$\begin{aligned}\mathbf{A}_{\mathbf{G},\mathbf{G}'} &\equiv \delta_{\mathbf{G},\mathbf{G}'}\left[\frac{\hbar^2}{2m}(\mathbf{k}+\mathbf{G})^2-\mu\right]+\tilde{U}_{\mathbf{G}-\mathbf{G}'} \\ &\quad+\sum_{\mathbf{G}''}\phi_{\mathbf{G}''-\mathbf{G}'}\phi_{\mathbf{G}-\mathbf{G}''}\tilde{V}_{\mathbf{k}+\mathbf{G}''} \\ \mathbf{B}_{\mathbf{G},\mathbf{G}'} &\equiv -\sum_{\mathbf{G}''}\phi_{\mathbf{G}''-\mathbf{G}'}\phi_{\mathbf{G}-\mathbf{G}''}\tilde{V}_{\mathbf{k}+\mathbf{G}''}\end{aligned} \tag{2.33}$$

Because of the fact that the $\mathbf{G}$ vectors are those defining the mesh in Fourier space, if we sample the simulation domain with n_r points along each direction in real space, the matrices $\mathbf{A}$ and $\mathbf{B}$ have dimensions $n_r^3 \times n_r^3$, which implies that the system 2.32 has dimensions $2(n_r^3 \times n_r^3)$, which makes it computationally exprensive for fine meshes. For instance, a typical 3D mesh of 48^3 points, would imply the diagonalization of a matrix of dimension (221184×221184). In double precision, to store one number, that is one entrance of the matrix, one needs 8 bytes, so that to store such a matrix we would need more than $300GB$ of RAM, and so cannot even be built in a commercial computer. Moreover, even if the two matrices $\mathbf{A}$ and $\mathbf{B}$ are separately hermitian, the complessive system 2.32 is not, so that one cannot use efficient algorithms for the diagonalization, that for example exists for Hermitian matrices (like, for example, the Lanczos method). The only possible simplification comes from the possibility of defining a system with the same eigenvalues, but of half size, namely

$$(\mathbf{A}-\mathbf{B})(\mathbf{A}+\mathbf{B})(\mathbf{u}+\mathbf{v}) = (\hbar\omega)^2(\mathbf{u}+\mathbf{v}) \tag{2.34}$$

which simplify the computation of the excitation spectrum.
Finally, adding the LHY correction in the form 1.47, in this formalism results in the following modification of the matrices $\mathbf{A}$ and $\mathbf{B}$

$$\begin{aligned}\mathbf{A}_{\mathbf{G},\mathbf{G}'} &\to \mathbf{A}_{\mathbf{G},\mathbf{G}'}+\frac{3}{2}\gamma(\epsilon_{dd})\tilde{\mathbf{L}}_{\mathbf{G}-\mathbf{G}'} \\ \mathbf{B}_{\mathbf{G},\mathbf{G}'} &\to \mathbf{B}_{\mathbf{G},\mathbf{G}'}-\frac{3}{2}\gamma(\epsilon_{dd})\tilde{\mathbf{L}}_{\mathbf{G}-\mathbf{G}'}\end{aligned} \tag{2.35}$$

where the matrix elements of $\tilde{\mathbf{L}}_{\mathbf{G}-\mathbf{G}'}$ are defined through

$$n^{\frac{3}{2}}(\mathbf{r}) = \sum_{\mathbf{G}}\tilde{\mathbf{L}}_{\mathbf{G}}e^{i\mathbf{G}\cdot\mathbf{r}} \tag{2.36}$$

So, when we consider the reduced system 2.34, we only need to add to the matrix $(\mathbf{A}-\mathbf{B})$ the term $3\gamma(\epsilon_{dd})\tilde{\mathbf{L}}$.
To sum up, to study the elementary excitations of the condensate by solving the Bogoliubov-de Gennes equations in conditions in which quantum fluctuations are important, we need to construct the matrices $\mathbf{A}$, $\mathbf{B}$ and $\mathbf{L}$, correct the matrix $\mathbf{A}$-$\mathbf{B}$ by adding $3\gamma(\epsilon_{dd})\tilde{\mathbf{L}}$, and diagonalize the system 2.34. Notice that, to construct these matrices, we need the ground state wave function, so that we need, in advance, to perform also a propagation in imaginary time to find it. Moreover, the system is hard to diagonalize not only because of its

dimensions, but also because it does not possesses any particular symmetry. Thus, we need always to use minimal meshes, using the smallest number of points which is enough for an accurate solution of the problem (note that, if the system is homogeneous along a certain direction, then the density is described by only one Fourier component along that direction, and so we can sample that direction using only one point. This will be extremely usefull in the following).
Before studying the system we are interested in by using the numerical methods presented in this chapter, we present a simplified variational approach to the problem, based on a gaussian ansatz for the density along the confinement directions, set as the z (polarization) and y direction, and uniform along x.

Chapter 3

Variational study of a dipolar BEC confined in a ring geometry

As stated in the introduction, the present thesis is mainly concerned with the study a dipolar BEC confined in a ring geometry. We have been inspired by a recent experiment [19], in which the authors show that a roton mode is detected in a dipolar BEC of ^{166}Er confined in a prolate, cygar-shaped trap, after the scattering length of the initially stable BEC is quenched to a certain small value (as compared with the dipolar length a_{dd} of erbium, which is $65.5a_0$). The roton mode manifest itself in the measured momentum distribution along the main axis of the trap, with the appearance of two symmetrical peaks at finite momentum. This experiment implies that, for a quasi-1D dipolar BEC, it is possible to soften the roton mode, as explained in chapter 1, and thus the system can substain a modulation of the density in its ground state.
In order to simulate a perfectly periodical structure along one dimension, we confine the dipoles, aligned along the z-axis, inside a *ring* geometry, in which a finite periodic system can be accomodated. Moreover, we use an approximation of this geometry, in the form of a straight "tube" along the x-axis, and "match" the two extrema of the tube by enforcing periodic boundary conditions

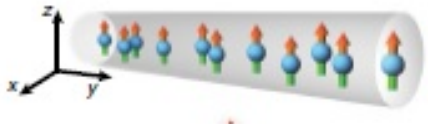

Figure 3.1: Schematic representation of the geometry considered

We thus perform a simplified variational study of the problem, based on a gaussian ansatz for the density along the confinement directions, and uniform along the tube. This way, we gain an insight on the qualitative behaviour of the system as the interaction parameters are modified.

3.1 Energy functional

We consider the energy functional described in chapter 1, obtained in our Density Functional description

$$\begin{aligned} E[n] = &\int d\mathbf{r}\frac{\hbar^2}{2m}|\nabla\sqrt{n(\mathbf{r})}|^2 \\ &+ \int d\mathbf{r}V_{ext}(\mathbf{r})n(\mathbf{r}) \\ &+ \frac{1}{2}\int d\mathbf{r}d\mathbf{r}'n(\mathbf{r})V(\mathbf{r}-\mathbf{r}')n(\mathbf{r}') \\ &+ \frac{2}{5}\gamma(\epsilon_{dd})\int d\mathbf{r}n(\mathbf{r})^{\frac{5}{2}} \end{aligned} \tag{3.1}$$

where V is the pseudo-potential 1.27. Then, we make the following gaussian ansatz for the density profile

$$n(\mathbf{r}) = \frac{n_0}{2\pi\sigma_y\sigma_z}e^{-\frac{1}{2}\left[\left(\frac{y}{\sigma_y}\right)^2+\left(\frac{z}{\sigma_z}\right)^2\right]} \tag{3.2}$$

where $n_0 = N/L$ is the linear density along the x-axis, N is the total number of particles and L is the length of the tube. Moreover, we use, as variational parameters, the harmonic lengths σ_y and σ_z. Inserting this in the energy functional 3.1 leads to the following expression for the energy per particle as function of the two harmonic lengths σ_y and σ_z

$$\begin{aligned} \frac{E[\sigma_y,\sigma_z]}{N} =&\frac{\hbar^2}{8m}\left(\frac{1}{\sigma_y^2}+\frac{1}{\sigma_z^2}\right) \\ &+ \frac{m}{2}\left(\omega_y^2\sigma_y^2+\omega_z^2\sigma_z^2\right) \\ &+ \frac{\hbar^2}{2m}\frac{n_0a(1-\epsilon_{dd})}{\sigma_y\sigma_z} \\ &+ \frac{\hbar^2}{2m}\frac{6\epsilon_{dd}n_0a}{\pi L}\int d\mathbf{k}\frac{sin^2\left(\frac{k_xL}{2}\right)}{k_x^2}\frac{k_z^2}{k_x^2+k_y^2+k_z^2}e^{-(\sigma_y^2k_y^2+\sigma_z^2k_z^2)} \\ &+ \frac{4}{25}\gamma(\epsilon_{dd})\left(\frac{n_0}{\pi\sigma_y\sigma_z}\right)^{\frac{3}{2}} \end{aligned} \tag{3.3}$$

where the integral term comes from the evaluation of the dipole-dipole interaction energy in Fourier space, and cannot be evaluated analitically.
To extract usefull informations from this energy functional, we need to fix the trapping parameters. In particular, we can choose the trapping frequencies in the typical range

of the experiments [19, 14, 36], and a reasonable length of the tube. In particular, we fix

$$\begin{aligned} \omega_y &= 2\pi(600)Hz \\ \omega_z &= 2\pi(600)Hz \\ L &= 10\mu m \end{aligned} \tag{3.4}$$

and minimize the energy functional 3.3 with respect to σ_y and σ_z, for a fixed choice of n_0 and ϵ_{dd}. We stress that this particular choice does not compromise the generality of the results. With a different choice of the trap geometry, one finds qualitatively the same physics, but just in a different range of the free parameters n_0 and ϵ_{dd}.
Thus, the energy functional 3.3 is numerically minimized with respect to σ_y and σ_z, using a steepest descent algorithm, for different values of n_0 and ϵ_{dd}. The minima of the energy are then reported in the plane n_0-ϵ_{dd}, as shown in the following figure

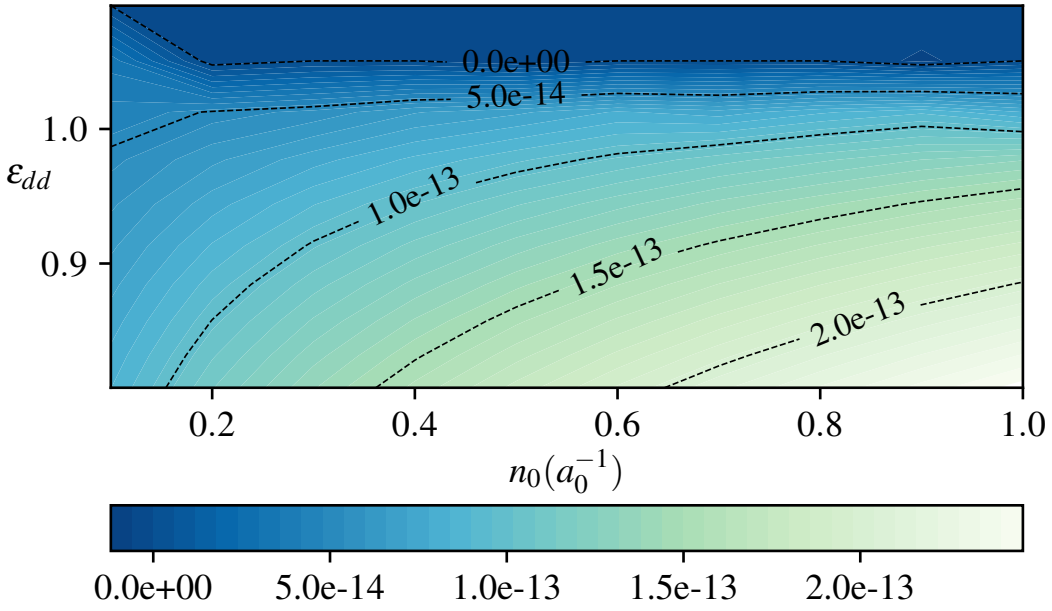

Figure 3.2: Minima of the energy as a function of n_0 and ϵ_{dd}. Lines of equal energy are also reported. Energies are expressed in atomic units

It is clear that, for a fixed linear density, increasing the dipolar parameter leads to a reduction in the energy, until the line of zero energy per particle is crossed. When this happens, the energy per particle becomes negative, and we expect to find stable self-bound states in that part of the diagram. However, this aspect cannot be studied in the present variational approach, as it is too much simplified. Nonetheless, in case of positive energy, some other interesting qualitative features can be derived.
For a fixed value of n_0, as the system gets closer to the zero-energy line by increasing ϵ_{dd} (by reducing the scattering length, since a_{dd} is fixed), one expects that dipolar effects

becomes more and more important. In this variational model, this aspect can be studied by looking at the aspect ratio of the condensate, that can be defined as

$$\lambda = \frac{\sigma_z}{\sigma_y} \tag{3.5}$$

Because of the fact that the dipoles are polarized along the z axis, we expect that the aspect ratio increases with increasing ϵ_{dd}, as the system tends to become elongated along the polarization direction. At the same time, it is reasonable to expect that the peak density, defined as the density at the center of the trap

$$\rho_{max} = \frac{n_0}{2\pi\sigma_y\sigma_z} \tag{3.6}$$

increases as one gets close to the instability line. So, we calculate the aspect ratio of the condensate and the peak density from the values of σ_y and σ_z that minimize the energy, for a fixed value of n_0 and increasing ϵ_{dd}. The results are shown in figure 3.3, from which it is clear that the numerical results are compatible with what is expected.

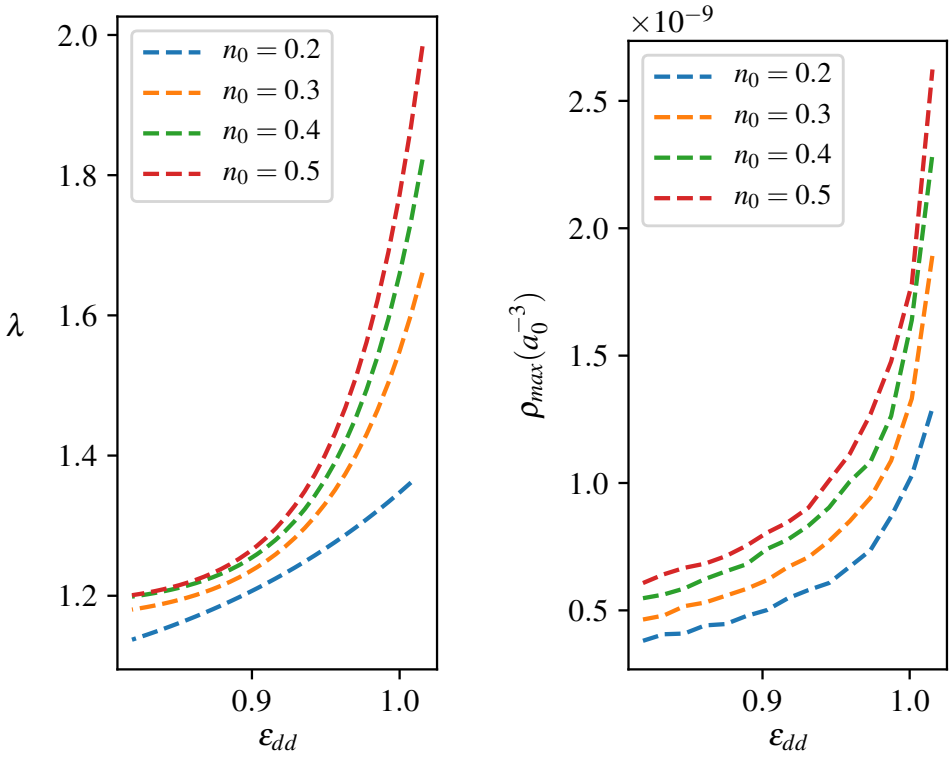

Figure 3.3: Aspect ratio and peak density for different values of n_0 as function of ϵ_{dd}, with n_0 in units of a_0^{-1}

Moreover, from figure 3.3, we can see that λ and ρ_{max} increase exponentially with ϵ_{dd}, meaning that, as we get close to the instability line the system becomes more and more

dense at the center of the trap and elongated along the polarization axis.

3.2 Effective interaction between dipolar atoms confined in a ring

From this variational model we can extract another interesting information. Following the procedure shown in [56], we can calculate an effective interaction potential for the dipoles in 1D by starting with a gaussian ansatz of the form

$$n(\mathbf{r}) = \frac{n(x)}{2\pi\sigma_y\sigma_z} e^{-\frac{1}{2}\left[\left(\frac{y}{\sigma_y}\right)^2+\left(\frac{z}{\sigma_z}\right)^2\right]} \tag{3.7}$$

that is, we allow the density to be also non uniform along the x-axis, and writing the energy functional as

$$E[n] = \int dx V_{eff}(x) n^2(x) \tag{3.8}$$

where $V_{eff}(x)$ comes from the integration along y and z, and can be interpreted as an effective one dimensional interaction potential. So, inserting 3.7 into the energy functional 3.3, we find that the effective potential in Fourier space can be written as

$$\tilde{V}_{eff}(k_x) = \frac{g}{4\pi\sigma_y\sigma_z}\left\{1 - \epsilon_{dd}\left[1 - 3I(k_x, \sigma_y, \sigma_z)\right]\right\} \tag{3.9}$$

whith

$$I(k_x, \sigma_y, \sigma_z) = \int \frac{dk_y dk_z}{(2\pi)^2} \frac{k_x^2}{k_x^2 + k_y^2 + k_z^2} e^{-(k_y^2\sigma_y^2 + k_z^2\sigma_z^2)} \tag{3.10}$$

For a homogeneous 1D system interacting through the potential 3.9, the excitation spectrum is given by 1.36, that is

$$\epsilon_{k_x} = \sqrt{\frac{\hbar^2 k_x^2}{2m}\left[\frac{\hbar^2 k_x^2}{2m} + 2n_0\tilde{V}_{eff}(k_x)\right]} \tag{3.11}$$

Thus, we can again fix the trap geometry as before, fix the values of n_0 and ϵ_{dd}, calculate the values of σ_y and σ_z that minimize the energy, and insert them into the dispersion relation 3.11, finding and estimate for the qualitative behavior of the excitation spectrum as the various parameters are changed. In particular, this procedure has been followed for the fixed choice of $n_0 = 0.5a_0^{-1}$ and increasing ϵ_{dd}, finding the results shown in the following figure

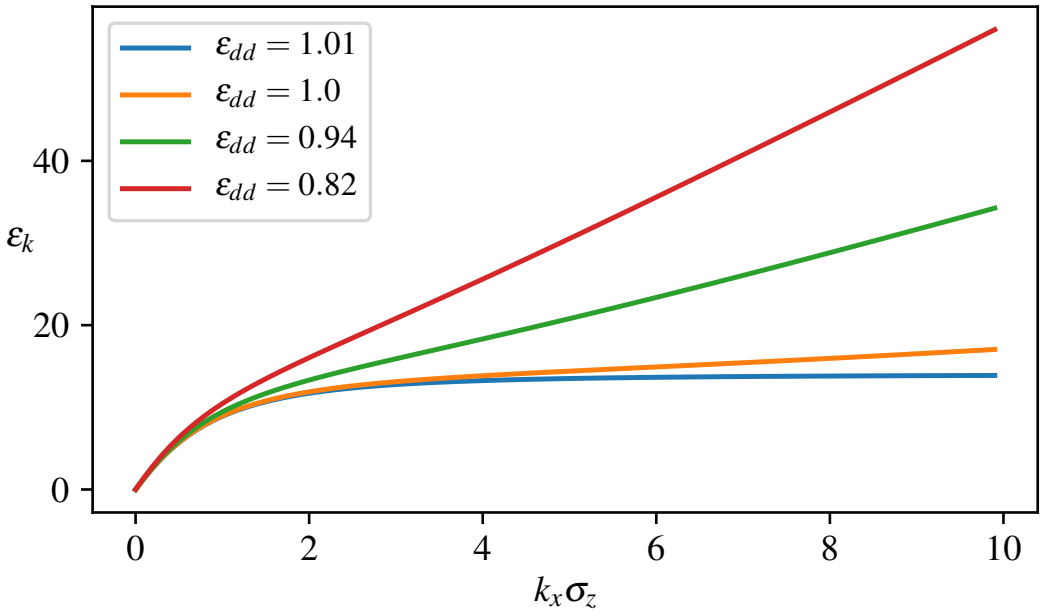

Figure 3.4: Excitation spectrum 3.11 for different values of ϵ_{dd}, obtained for $n_0 = 0.5a_0^{-1}$. The energy is in units of $\frac{\hbar^2}{2m\sigma_z^2}$

It is clear that, as we get close to the zero-energy line, the excitation spectrum softens, meaning that possibly a roton minimum can form after the line is crossed. However, in this simple model it is not possible to actually check if the roton minimum forms or not, as beyond the zero-energy line this model is not affordable anymore. For this reason, in the following sections, these aspects will be explored using the proper instruments presented in chapter 2.

Chapter 4

Formation of the roton minimum

As shown at the end of the previuos chapter, it is possible that the system under study develops a roton minimum in the excitation spectrum in a condition in which dipolar effects becomes predominant. This aspect cannot be studied in the variational model presented previously, but can be explored by solving the Bogoliubov-de Gennes equations 1.32. We expect that the roton mode will manifest itself in the excitation spectrum, and that the roton gap can be reduced by further enhancing dipolar effects. The possibility of tuning the roton gap to zero opens up the possibility of the formation of a modulation of the ground state density profile along the x-axis, and thus to the formation of a system that shows hallmarks of supersolid behaviour, as explained in chapter 1.

4.1 Excitation spectrum of the homogeneous system

To recall the main results, the fundamental point is to construct the matrices $\mathbf{A}$, $\mathbf{B}$ and $\mathbf{L}$ using 2.33 and 2.36, and diagonalize the system 2.34 after adding to $\mathbf{A}-\mathbf{B}$ the term $3\gamma(\epsilon_{dd})\mathbf{L}$ that takes into account beyond-mean-field effects. As stated before, this procedure is computationally very expansive for a 3D mesh, as the dimensions of the matrices are of $n_r^3 \times n_r^3$, where n_r is the number of points used to sample each direction in real space. However, we can simplify the problem in a quasi-1D geometry, using the fact that the system is homogeneous along x, and so its Fourier component can be represented by just a single point. Thus, we can, at the same time, use a fine mesh in the y-z plane.
As shown in the variational study, once we fix the trap geometry, the energy depends only on n_0 and ϵ_{dd}. So, we fix a certain value of n_0 and ϵ_{dd}, calculate the ground state wave function $\phi(\mathbf{r})$, construct the matrices $\mathbf{A}$, $\mathbf{B}$ and $\mathbf{L}$, and diagonalize the system 2.34, as explained in chapter 2. The typical results are shown in figure 4.1 for modes propagating along the x-axis

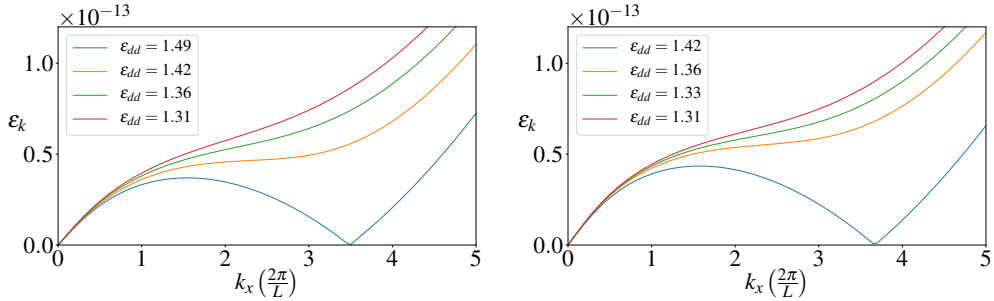

Figure 4.1: Excitation spectrum for the case $n_0 = 0.1a_0^{-1}$ (left panel) and $n_0 = 0.2a_0^{-1}$ (right panel), for different values of ϵ_{dd}. Energies are in atomic units

It is clear that, for a fixed n_0, as we increase ϵ_{dd}, the excitation spectrum develops a roton minimum, that softens as we further increase the dipolar interaction. For a certain value of ϵ_{dd}, the roton minimum touches the k_x axis, so that, in this condition, a modulation of the density profile along the x-axis with wavelength $\lambda = \frac{2\pi}{k_x}$ costs no energy, and thus can spontaneously develop even in the ground state. The value of ϵ_{dd} at which this happens decrease with n_0, meaning that as we increase the initial density, it is easier to destabilize the initial homogeneous system.
In figure 4.2 we report the same results for higher values of n_0.

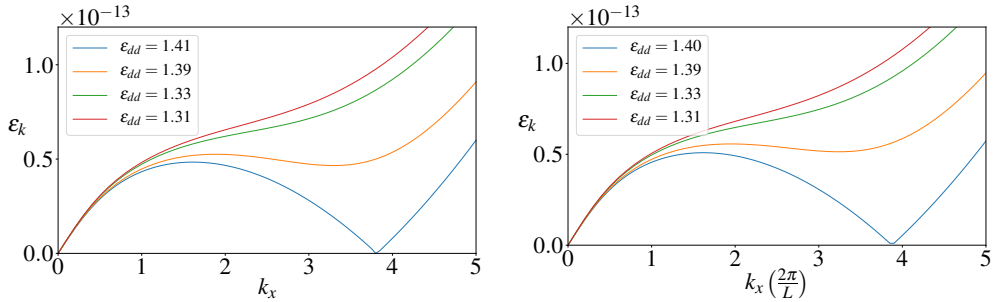

Figure 4.2: Excitation spectrum for the case $n_0 = 0.3a_0^{-1}$ (left panel) and $n_0 = 0.4a_0^{-1}$ (right panel), for different values of ϵ_{dd}. Energies are in atomic units

Comparing these results with those of figure 4.1, we notice that the critical value k_x^c of k_x at which the roton gap disappears weakly increases with n_0. This aspect is in qualitative agreement with what is found in [19], in which the authors, using a variational ansatz based on Thomas-Fermi approximation (that is, using a *parabolic* ansatz for the density profile along the confinement directions), find that k_x^c scales as the inverse of l_z, where l_z is the extension of the BEC along the polarization direction, and which in turn decreases if n_0 is increased.
If we further increase ϵ_{dd} we obtain the results shown in figure 4.3

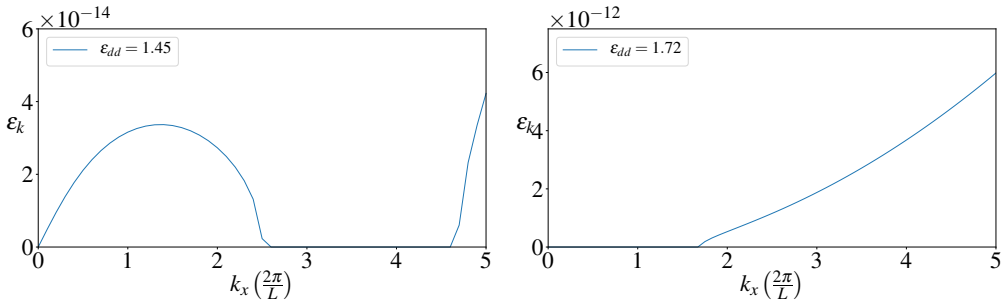

Figure 4.3: Dispersion relations for $n_0 = 0.2a_0^{-1}$ for higher values of ϵ_{dd}. The left panel shows the typical spectrum of a roton instability, while the right panel shows the spectrum of a phonon instability. Energies are in atomic units

We can see that, as ϵ_{dd} is increased beyond the value at which the roton gap disappears, the roton minimum becomes imaginary, meaning that the frequencies of the oscillations acquire an imaginary part and thus can destabilize the system. In this condition, we expect the density to be strongly modulated along the x-axis.
Finally, increasing ϵ_{dd} even further, we see that also the phonon part of the spectrum becomes imaginary, and so long-wavelength modes makes the system unstable. In this conditions, even in presence of the LHY correction, the system collapse and no stable ground-state can be found.
The results presented in this chapter suggests that, as we increase ϵ_{dd}, a density modulation will spontaneously develop in the ground state of the system, as consequence of the softening of the roton mode. The detailed study of such modulated structure will be the subject of the following chapter.

Chapter 5

Supersolid behaviour

From the results of the previous chapter, we now expect that a calculation of the ground state in a condition in which the roton gap disappears will give a density profile modulated along the x-axis. We will then study the properties of this modulated structure, in order to find if it hosts a supersolid phase.

5.1 Modulated superfluid

We now perform ground calculations of the system, for different values of ϵ_{dd}, in the geometry defined in 3.4, that is a tube geometry along the x-axis, with periodic boundary conditions enforced, and with a tight confinement in the y-z plan. In order to do so, we evolve the extended NLGPE 1.46, that includes also beyond-mean-field effects, in imaginary time to find the ground state of the system. The initial wave function is chosen in the form of a gaussian profile along the directions of confinement, and a constant plus some random noise in the x-direction.
Consider the case of $n_0 = 0.2a_0^{-1}$, for which the excitation spectrum at different values of ϵ_{dd} is reported in figure 4.1. The roton gap becomes zero for $\epsilon_{dd} = 1.42$, and the roton minimum touches the k_x-axis for $k_x \simeq 3.61\frac{2\pi}{L}$, corresponding to a wavelength of $\lambda \simeq 5.2 \times 10^4 a_0$. This period is relative to the modulation of the wave function, so that the density, which is given by its square modulus, will oscillate with a wavelength of $\lambda \simeq 2.6 \times 10^4 a_0$ (or about 7 oscillations of the density in the geometry defined in 3.4). We thus calculate the ground state of the system for different values of ϵ_{dd}, and the results are shown in figure 5.1.

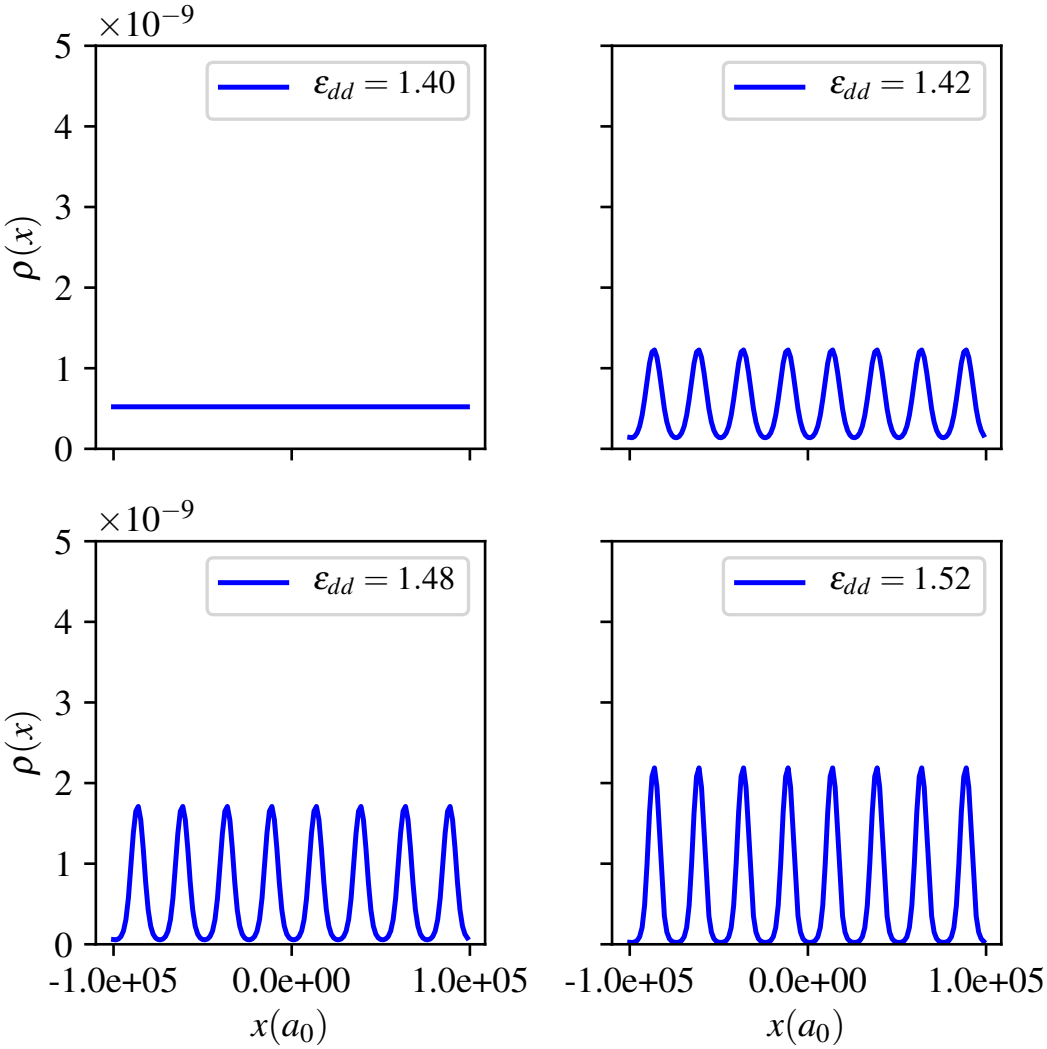

Figure 5.1: Density profile along the x-axis for $n_0 = 0.2$ and different values of ϵ_{dd}

We can see that the x-profile of the density is homogeneous for $\epsilon_{dd} < 1.42$, when the roton gap is still different from zero. However, exactly as $\epsilon_{dd} = 1.42$, the density along the x-axis becomes modulated with the expected wavelength (we report that in some systems, as shown for example in [47], a modulation of the density appears even *before* the roton gap disappears). Moreover, as we further increase ϵ_{dd}, the peaks of the density becomes more and more localized and higher, i.e. the peak density increase as dipolar effects are enhanced. The inclusion of the LHY correction in the simulations is fundamental in these conditions, as, without the inclusion of quantum fluctuations, the density profiles collapse even for much smaller values of ϵ_{dd}. Notice also that the peaks of the density are not well separated, meaning that, between one peak and the adjacent one, there is still a non-zero fraction of the condensate. This aspect appears more clear if we look at

the contour plot of the integrated density along the z-axis, defined as

$$n_z(x,y) = \int dz n(x,y,z) \tag{5.1}$$

and which is an observable quantity in experiments. It is reported in figure 5.2 for different values of ϵ_{dd}

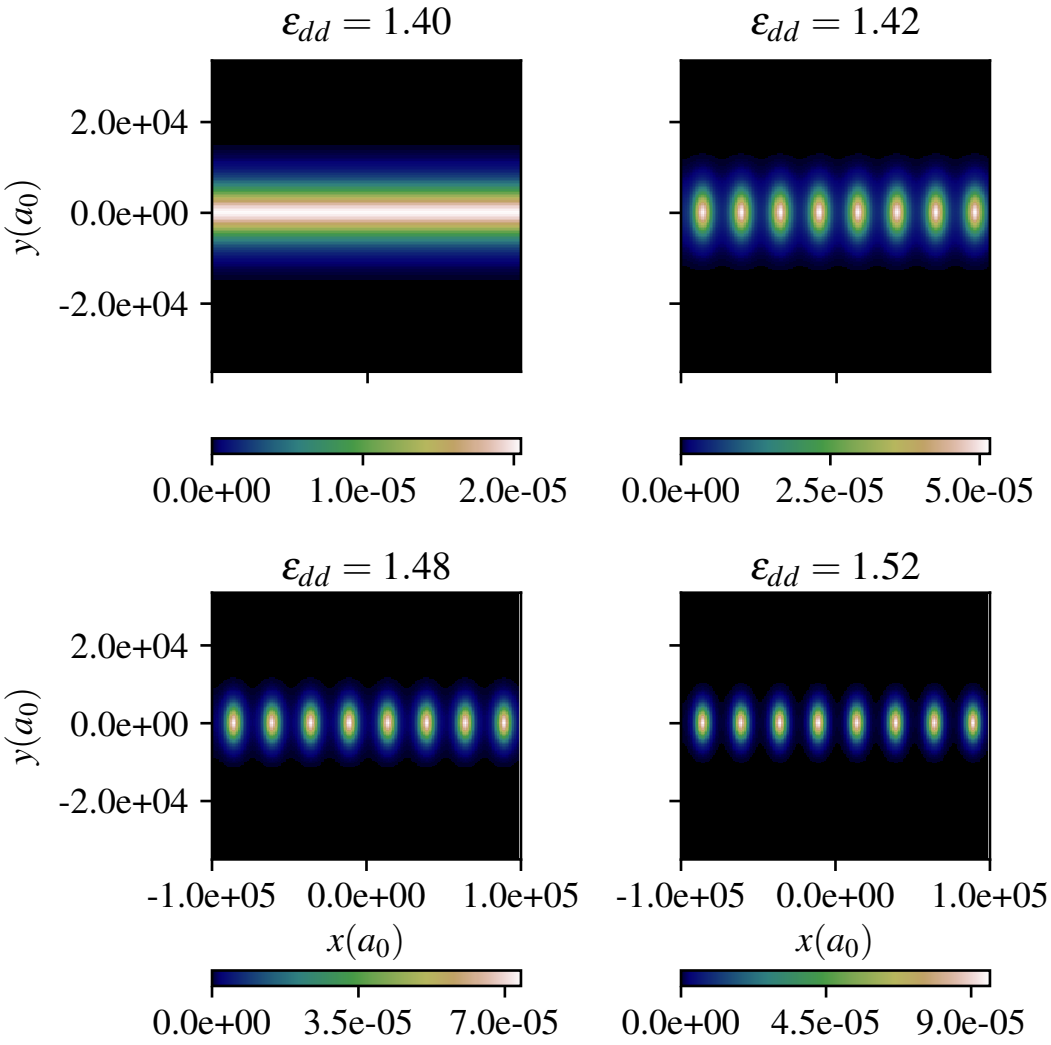

Figure 5.2: Integrated density $n_z(x,y)$ for different values of ϵ_{dd}

It is now clear that, as the roton gap becomes zero, the system spontaneously breaks the continuous translatioanl symmetry along the x-axis. The ground state of the system is then formed by an ordered array of denser clusters of atoms immersed in a dilute superfluid background. We notice also that, if we further enhance the dipolar interaction

by increasing ϵ_{dd}, the superfluid background tends to disappear, while the peaks of the density becomes higher and higher. So, even if this system is extremely dilute, it is possible that it shows the hallmarks of supersolid behaviour, and in particular: (i) a finite Non Classical Inertia (NCI), as described in chapter 1, and (ii) a gapless Goldstone mode in addition to the usual phonon mode.

5.2 Non Classical Inertia

We first calculate the superfluid fraction, analogous to NCI, according to 1.51. To recall the main result, we consider the extended NLGPE 1.46 for a system that translates with velocity v_x along the x-axis, that is

$$\mu\phi = \left(\hat{H} + i\hbar v_x \frac{\partial}{\partial x}\right)\phi \tag{5.2}$$

where $\hat{H}$ contains both mean-field and beyond-mean-field terms. We then solve the equation using imaginary time propagation, and calculate the superfluid fraction according to 1.51, that is

$$f_s = 1 - \frac{\langle \hat{\mathbf{P}} \rangle}{Nmv} \tag{5.3}$$

where $\langle \hat{\mathbf{P}} \rangle$ is the expectation value of the momentum, and N is the total number of particles. We repeat the calculation for different values of ϵ_{dd}, and the results are shown in figure 5.3

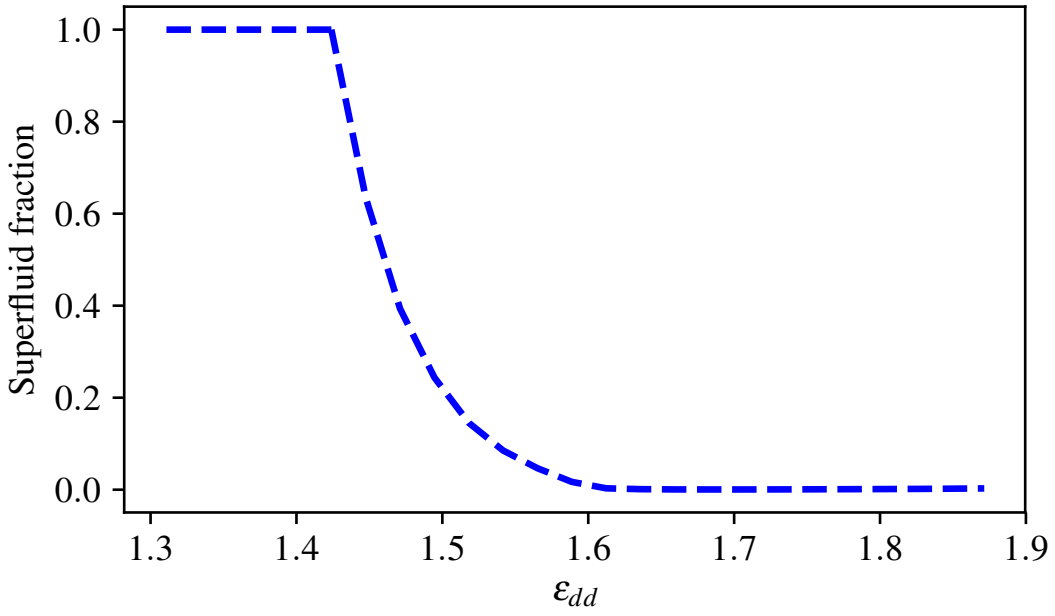

Figure 5.3: Superfluid fraction for $n_0 = 0.2a_0^{-1}$ as function of ϵ_{dd}

We see that that the superfluid fraction is equal to 1 for $\epsilon_{dd} < 1.42$, when the system is homogeneous, while it begins to decrease quickly for $\epsilon_{dd} > 1.42$ and becomes null at $\epsilon_{dd} \simeq 1.6$. This means that, for $1.42 < \epsilon_{dd} < 1.6$, not all the particles participate to the translational motion of the system. This can be interpreted as a proof of the fact that a finite superfluid fraction is detached from the "crystal" structure, and so it is not dragged by its motion. The inertia of the system under study is thus non-classical, as only a finite fraction of the system is influenced by the motion of the container. We now study the final signature of supersolid behaviour in the system under study, namely the appearance of an additional gapless mode beside the usual phonon mode.

5.3 Additional Goldstone mode

Following the results of the previous section, we fix $\epsilon_{dd} = 1.45$, value at which the superfluid fraction is about 0.6, and compute the full excitation spectrum of the excited system in 3D solving the BdG equations. In order to reduce the computational effort for this operation, we isolate one period along the x-direction, corresponding to one atomic cluster. A single cluster can be simulated using a mesh of about 28^3 points, so that the system 2.34 can be solved in a reasonable amount of time for each k_x. This way, we compute the excitation spectrum of the crystal cluster plus the superfluid fraction, and the results are shown in figure 5.4, where the first four modes are plotted into the first Brillouin zone, that is from $k_x = 0$ to $k_x = \pi/L$.

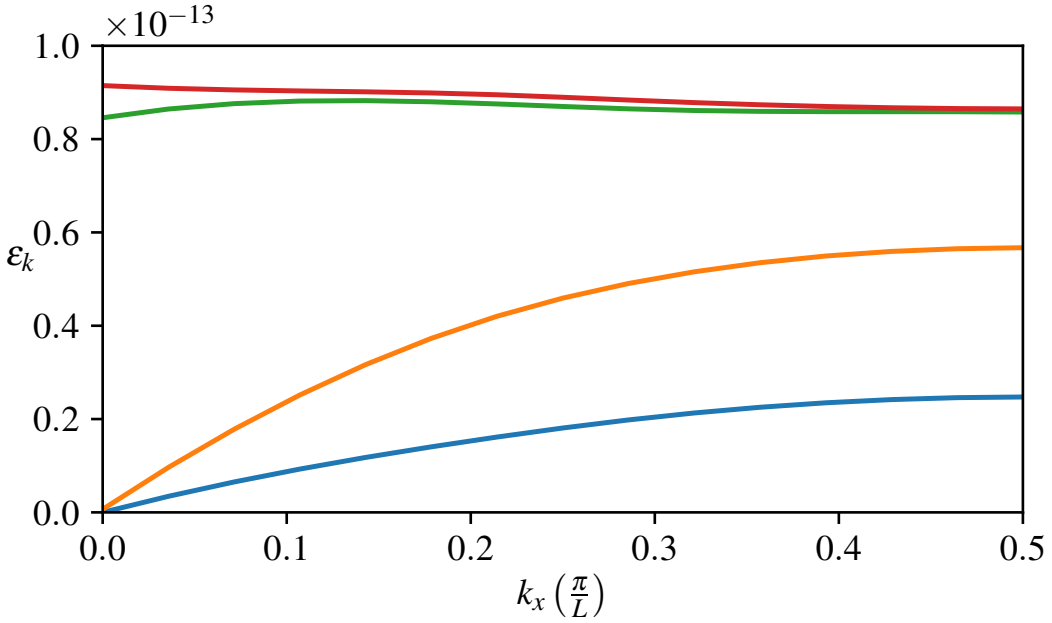

Figure 5.4: Excitation spectrum of the supersolid structure. Energies are in atomic units

Figure 5.4 shows the final proof of the presence of supersolidity in the system considered. In fact, we find two gapless modes for excitations alogn the x-axis, one corresponding to a standard phonon mode, and the other, at lower energy, corresponding to the Goldstone mode associated to the global phase coherence of the system. Moreover, we notice that there are also two higher energy, almost "flat" modes, in which the excitation energy is almost constant with k_x. This oscillation modes are called "breathing modes", and are associated to radial oscillations of the atomic clusters.
It is also interesting to look directly at the density and phase fluctuations for all the four modes. According to [48], they can be calculated as

$$\Delta\rho(\mathbf{r}) = \left\langle \delta\rho^\dagger(\mathbf{r})\delta\rho(\mathbf{r}) \right\rangle / |\phi(\mathbf{r})|^2 = \sum_{n,\mathbf{k}} |u_{n,\mathbf{k}} - v_{n,\mathbf{k}}|^2$$

$$\Delta\theta(\mathbf{r}) = \left\langle \delta\phi^\dagger(\mathbf{r})\delta\phi(\mathbf{r}) \right\rangle \times 4|\phi(\mathbf{r})|^2 = \sum_{n,\mathbf{k}} |u_{n,\mathbf{k}} + v_{n,\mathbf{k}}|^2$$

where $u_{n,\mathbf{k}}$ and $v_{n,\mathbf{k}}$ are the Bogoliubov amplitudes associated to a certain mode. It is then possible to isolate the contribution to $\Delta\rho$ and $\Delta\theta$ by computing the eigenvectors associated to a certain mode. The problem is that the system used to compute the eigenvalues 2.34 does not allow to compute directly the eigenvectors u and v. However, in the same way in which one can define the system 2.34, one can also define another system, with the same eigenvalues, as

$$(\mathbf{A}+\mathbf{B})(\mathbf{A}-\mathbf{B})(\mathbf{u}-\mathbf{v}) = (\hbar\omega)^2(\mathbf{u}-\mathbf{v}) \tag{5.4}$$

so that, combining the two systems, we can calculate the individual u and v. It is clear however that in this case the computational cost is two times the one required for the calculation of the eigenvalues. We did this for four selected values of k, two corresponding to the gapless modes at the boundary of the Brillouin zone, and two corresponding to the two breathing modes at $k_x = 0$. The results are shown in figure 5.5 for the two gapless modes. We can see that the lowest gapless mode contributes mainly to the phase fluctuation, while the second gapless mode contributes mainly to the density fluctuation. Thus, we are finally led to identify the first gapless mode to the Goldstone mode associated with the superfluid response of the system, or a phonon propagating in the phase.

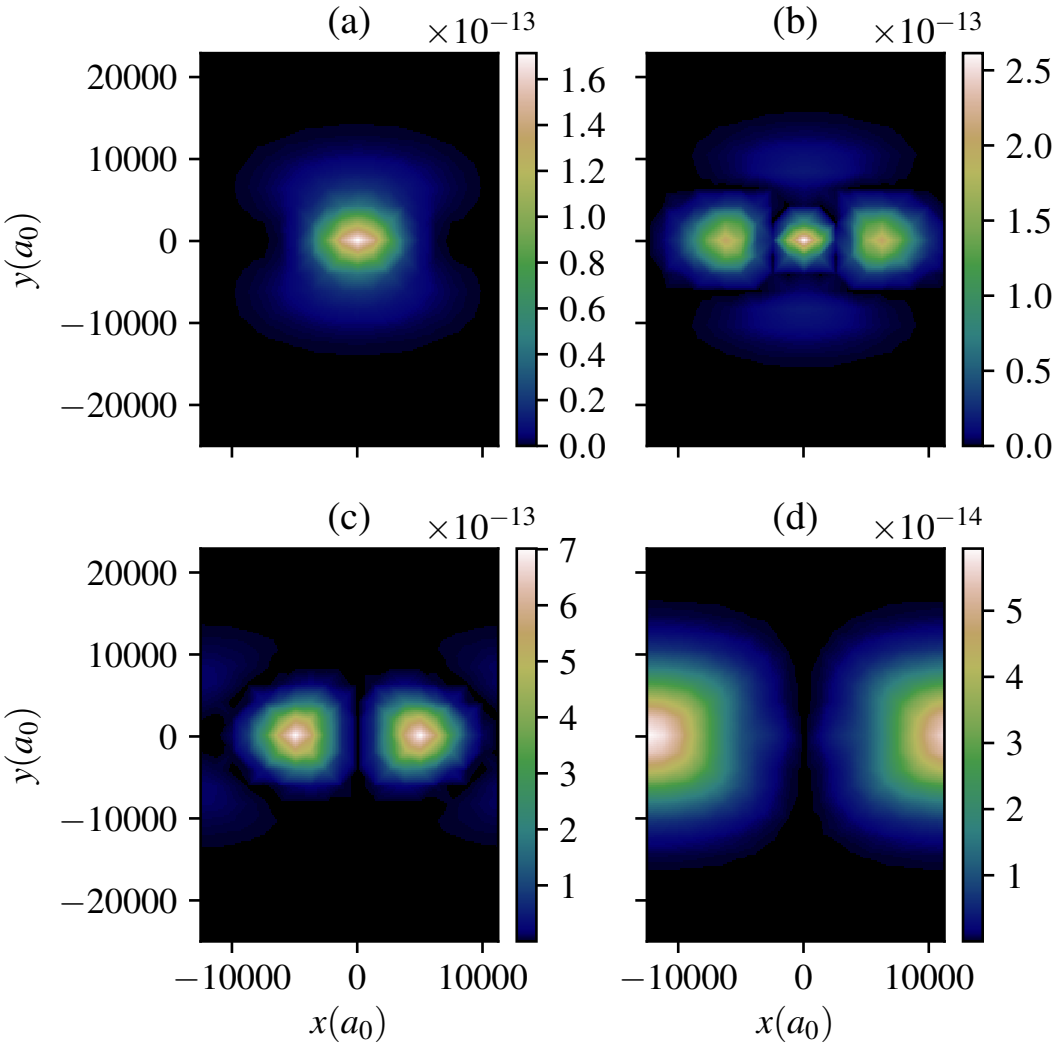

Figure 5.5: Density and phase fluctuations for the two gapless modes at $k_x = 0.5$. Figures (a)-(c) show the density fluctuation for the first and second gapless mode, while figures (b)-(d) shows the corresponding phase fluctuations

If we look instead at the two breathing modes, we find that both modes contributes heavily to both density and phase fluctuations, as shown in figure 5.6

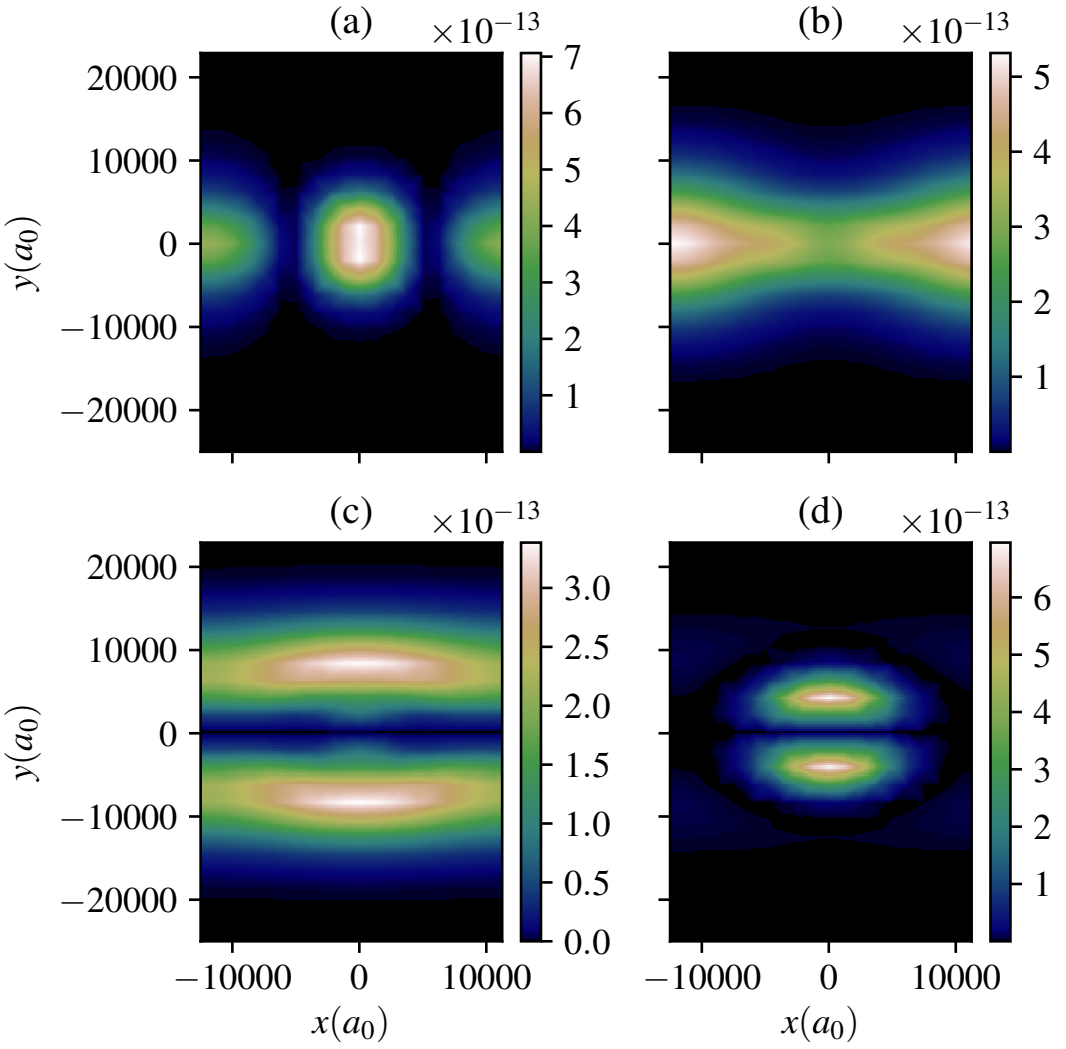

Figure 5.6: Density and phase fluctuations for the two optical modes at $k_x = 0$. Figures (a)-(c) show the density fluctuation for the first and second optical mode, while figures (b)-(d) shows the corresponding phase fluctuations

5.4 Destruction of the supersolid phase

It is interesting to study also what happens for higher values of ϵ_{dd}, when the superfluid fraction goes to zero. For this reason, we perform other similar simulations as those presented in the previous section, but for higher values of ϵ_{dd}. The results are shown in figure 5.7

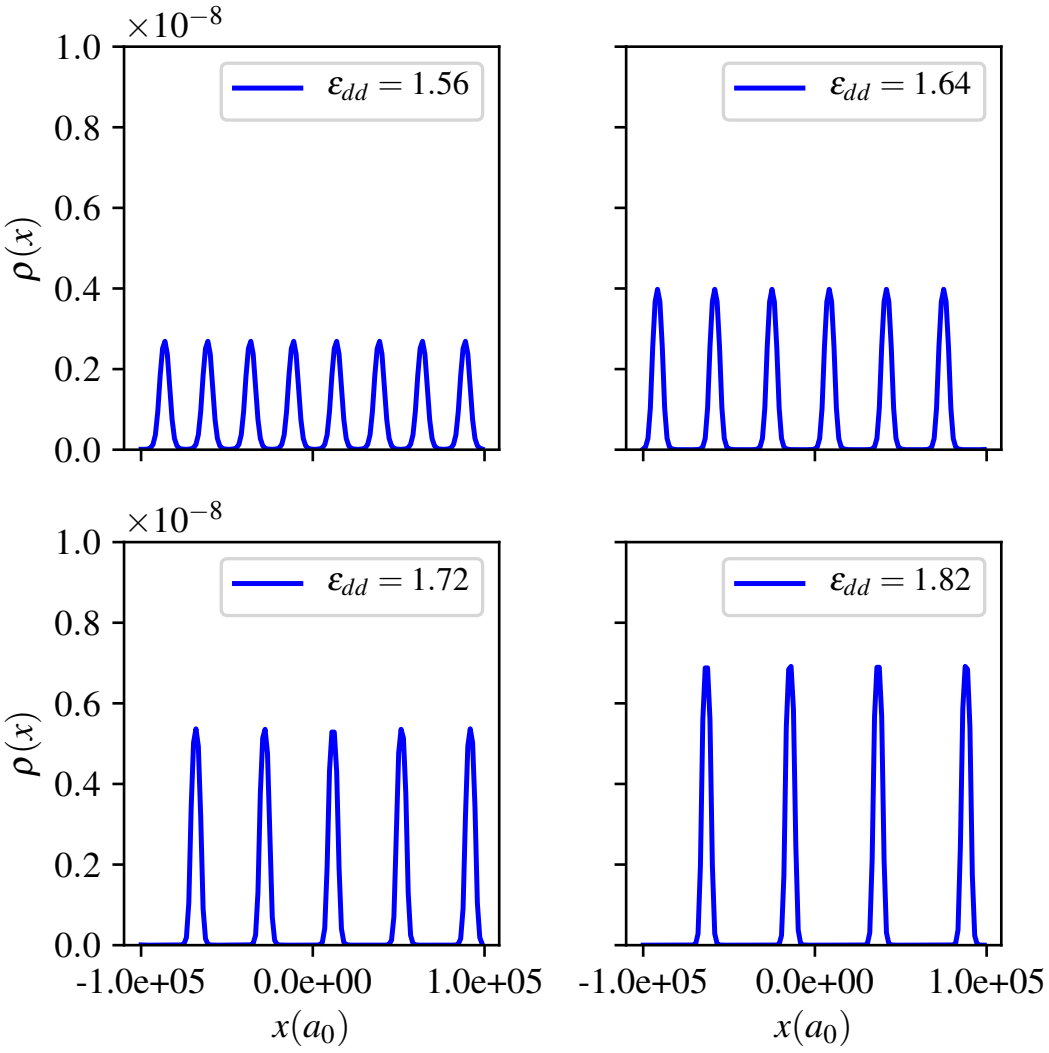

Figure 5.7: Density profile along the x-axis for $n_0 = 0.2$ and higher values of ϵ_{dd}. Units are the same as those used in figure 5.1

We see that, as we increase ϵ_{dd} beyond 1.62, the atomic clusters begin to merge, and their number is quickly reduced from 8 to 4 as ϵ_{dd} is increased from 1.64 to 1.82. Again, it is also usefull to look at the integrated density, reported in figure 5.8

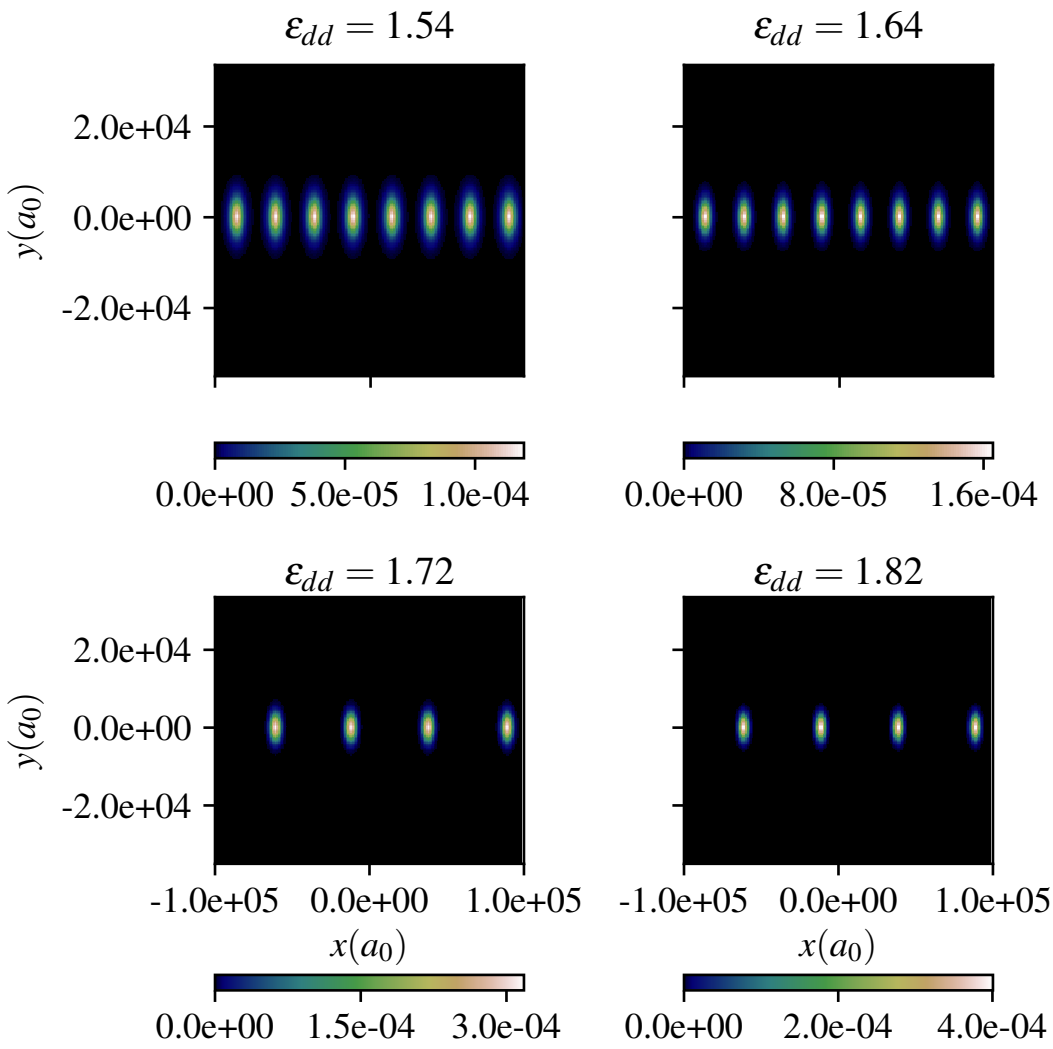

Figure 5.8: Integrated density $n_z(x, y)$ for higher values of ϵ_{dd}

This tendency of the atomic clusters to merge continues if we further increase ϵ_{dd}, until we reach a point in which the LHY correction is too high and the system collapses, with the density that becomes null everywhere except for the center of the trap, in which it shows a pronounced peak formed by only one point.
To have an insight on what is going on, it is usefull to look at the behaviour of the energy per particle of the system as function of ϵ_{dd}, which is shown in figure 5.9

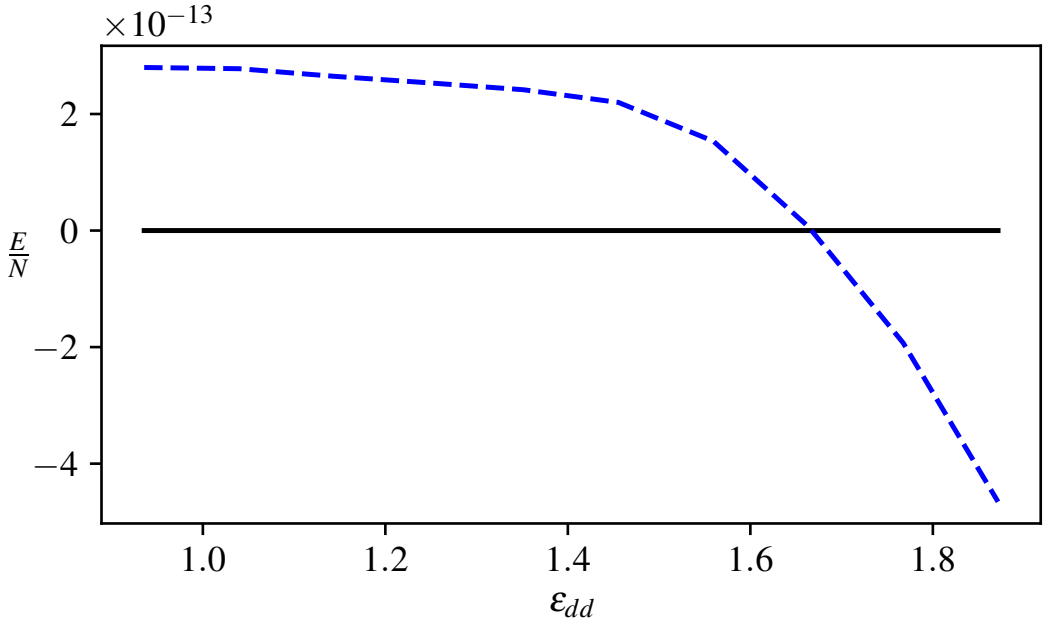

Figure 5.9: Energy per particle as function of ϵ_{dd}. Energy is in atomic units

We notice that, as the clusters begin to merge, the energy per particle becomes negative, and the value of ϵ_{dd} at which the energy changes sign corresponds to that at which the superfluid fraction becomes zero. The fact that the energy per particle becomes negative implies that the atomic clusters becomes self-bound, while the fact that the superfluid fraction becomes zero signals that the supersolid behaviour is suppressed.
A further proof of the suppression of the supersolid behaviour is given by the excitation spectrum of the system, which is reported in figure 5.10

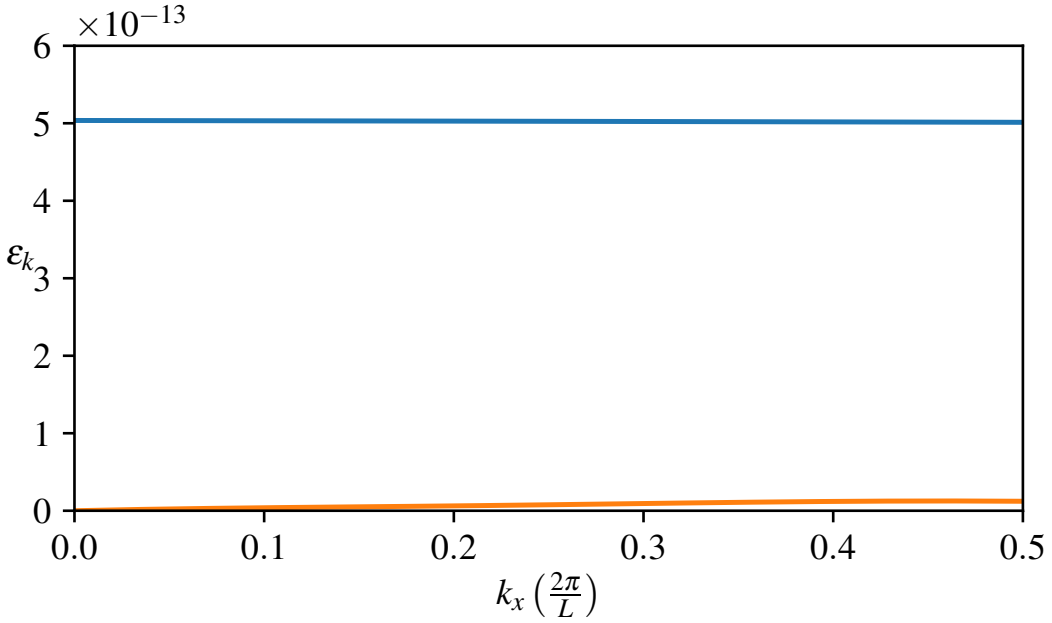

Figure 5.10: Excitation spectrum of the crystal cluster. Energies are in atomic units

We can see that now we have only one gapless mode, and the supersolid nature of the system is destroyed.
To gain a final insight on the nature of the self-bound clusters described above, it is usefull to look at the inverse compressibility of the system, defined as

$$k^{-1} = -V\frac{\partial P}{\partial V} = -V\frac{\partial E}{\partial V} \tag{5.5}$$

where V is the volume of the system, P is the pressure and E the total energy. This quantity is reported in figure 5.11 as function of ϵ_{dd}.

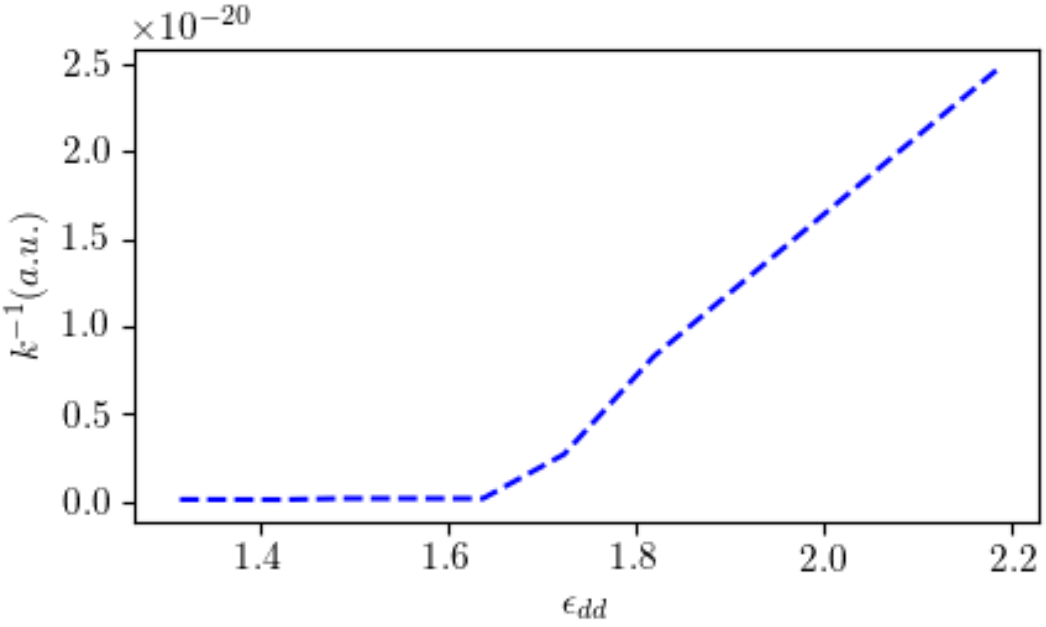

Figure 5.11: Inverse compressibility as function of ϵ_{dd}, expressed in atomic units

We see that, as the clusters become self-bound, the inverse compressibility increases quickly, meaning that the clusters behave as incompressible, liquid-like droplets, even if still extremely dilute if compared with an ordinary liquid.
We thus find that the suppression of the supersolid behaviour in our system, signaled by the disappearance of any superfluid background and of the gapless mode associated to the superfluid response of the system, is accompanied by the degeneration of atomic clusters into self-bound, liquid-like quantum droplets.

Chapter 6

Conclusions

In this thesis, we demonstrated, by means of numerical simulations based on Density Functional Theory, that in a dipolar BEC confined in a quasi-1D ring geometry, the softening of the roton mode leads to the formation of a modulated structure in the ground state of the system. The competition between mean-field attraction, due the partially attractive part of the dipolar interaction, and the beyond-mean-field repulsion given by the Lee-Huang-Yang correction, leads to the formation of a periodic structure of denser clusters of atoms, immersed in a dilute superfluid background. In these conditions, the system shows hallmarks of supersolidity, and in particular

- A finite, Non-Classical Translational Inertia, and
- An additional Goldstone gapless mode in the excitation spectrum.

Moreover, enhancing dipolar effects leads to the degeneracy of the atomic clusters into self-bound, liquid-like quantum droplets. When this happens, the supersolid behaviour is suppressed.
We remark that, even if we used the terms *supersolid* or *liquid*, we are still referring to systems of ultracold atoms, which are *extremely* dilute. To give some order of magnitude, ordinary matter has a typical density of $10^{22} atoms/cm^3$, while a BEC realized with atomic gases has a typical density of $10^{14} atoms/cm^3$. Nonetheless, a modulated structure made of denser atomic clusters immersed in a dilute superfluid shows features that allow to define these systems as *supersolids*.
Finally, the self-bound droplets that are formed when global phase coherence is destroyed, show liquid-like properties, such as very low compressibility (as compared with the initial gas). Their density is around one order of magnitude higher then that of the initial BEC, but once again it is orders of magnitudes lower then that of an ordinary liquid.

Appendix A

Derivation of the Bogoliubov dispersion relation

We stated in some previous chapter that the Bogoliubov dispersion relation for a homogeneous system of bosons interacting through the potential $V(\mathbf{r})$ is given by

$$\hbar\omega_{\mathbf{k}} = \sqrt{\frac{\hbar^2\mathbf{k}^2}{2m}\left(\frac{\hbar^2\mathbf{k}^2}{2m} + 2n_0\tilde{V}_{\mathbf{k}}\right)} \tag{A.1}$$

Recall the form of the BdG equations 1.32

$$\begin{aligned}
\hbar\omega u(\mathbf{r}) = \left[-\frac{\hbar^2}{2m}\nabla^2 - \mu + V_{ext}(\mathbf{r}) + \int d\mathbf{r}' V(\mathbf{r}-\mathbf{r}')|\phi(\mathbf{r}')|^2\right] u(\mathbf{r}) \\
+\phi(\mathbf{r})\int d\mathbf{r}' V(\mathbf{r}-\mathbf{r}')[\phi^*(\mathbf{r}')u(\mathbf{r}') - \phi(\mathbf{r}')v(\mathbf{r}')] \\
-\hbar\omega v(\mathbf{r}) = \left[-\frac{\hbar^2}{2m}\nabla^2 - \mu + \int d\mathbf{r}' V(\mathbf{r}-\mathbf{r}')|\phi(\mathbf{r}')|^2\right] v(\mathbf{r}) \\
+\phi^*(\mathbf{r})\int d\mathbf{r}' V(\mathbf{r}-\mathbf{r})[\phi(\mathbf{r}')v(\mathbf{r}') - \phi^*(\mathbf{r}')u(\mathbf{r}')]
\end{aligned} \tag{A.2}$$

For a homogeneous condensate, from the NLGPE equation 1.29 we find

$$\mu = n_0\int d\mathbf{r} V(\mathbf{r}-\mathbf{r}') \tag{A.3}$$

which simplifies the BdG equations into

$$\begin{aligned}
\hbar\omega u(\mathbf{r}) = -\frac{\hbar^2\nabla^2}{2m}u(\mathbf{r}) + \int d\mathbf{r}' V(\mathbf{r}-\mathbf{r}')n_0[u(\mathbf{r}') - v(\mathbf{r}')] \\
-\hbar\omega v(\mathbf{r}) = -\frac{\hbar^2\nabla^2}{2m}u(\mathbf{r})\int d\mathbf{r}' V(\mathbf{r}-\mathbf{r}')n_0[v(\mathbf{r}') - u(\mathbf{r}')]
\end{aligned} \tag{A.4}$$

We can now take the Fourier transform of both sides, and using the convolution theorem of Fourier transforms [57], we obtain

$$\begin{aligned} \hbar\omega u_{\mathbf{k}} &= \frac{\hbar^2\mathbf{k}^2}{2m}u(\mathbf{k}) + \tilde{V}_{\mathbf{k}}[u_{\mathbf{k}} - u_{\mathbf{k}}] \\ -\hbar\omega v_{\mathbf{k}} &= \frac{\hbar^2\mathbf{k}^2}{2m}v(\mathbf{k}) + \tilde{V}_{\mathbf{k}}[v_{\mathbf{k}} - u_{\mathbf{k}}] \end{aligned} \tag{A.5}$$

It is now easy to solve for both the excitation spectrum and the amplitudes. In particular, by adding and subtracting both equations side by side, we find

$$\begin{aligned} \hbar\omega(u_{\mathbf{k}} - v_{\mathbf{k}}) &= \frac{\hbar^2\mathbf{k}^2}{2m}(u_{\mathbf{k}} + v_{\mathbf{k}}) \\ \hbar\omega(u_{\mathbf{k}} + v_{\mathbf{k}}) &= (u_{\mathbf{k}} - v_{\mathbf{k}})\left[\frac{\hbar^2\mathbf{k}^2}{2m} + 2n_0\tilde{V}_{\mathbf{k}}\right] \end{aligned} \tag{A.6}$$

Substituting the first equation into the second, one then easily finds

$$\hbar\omega = \sqrt{\frac{\hbar^2\mathbf{k}^2}{2m}\left[\frac{\hbar^2\mathbf{k}^2}{2m} + 2n_0\tilde{V}_{\mathbf{k}}\right]} \tag{A.7}$$

that is exactly the Bogoliubov dispersion relation 1.36.

Appendix B

Fourier transform of the dipolar potential

In chapter bo we stated that the Fourier transform of the pseudo-potential 1.27 is given by

$$\tilde{V}_k = g\left[1 + \epsilon_{dd}(3cos^2\theta - 1)\right] \tag{B.1}$$

While it is very simple to calculate the Fourier transform of the contact pseudo-potential 1.25

$$\int d\mathbf{r} g\delta(r)e^{-i\mathbf{k}\cdot\mathbf{r}} = g \tag{B.2}$$

the Fourier transform of the dipole-dipole potential is instead harder to compute. Consider the form of the dipole-dipole potential

$$V_{dd}(\mathbf{r}) = \frac{C_{dd}}{4\pi}\frac{1 - 3cos^2\beta}{r^3} \tag{B.3}$$

where β is the angle between $\mathbf{r}$ and the z-axis. Let us define the Fourier transform as

$$\tilde{V}_{dd}(\mathbf{k}) = \int d\mathbf{r} V_{dd}(\mathbf{r})e^{-i\mathbf{k}\cdot\mathbf{r}} \tag{B.4}$$

and use spherical coordinates, with the z-axis axis this time along $\mathbf{k}$, the dipole moment $\mathbf{d}$ in the $y = 0$ plane, and let α be the angle between $\mathbf{k}$ and the polarization direction

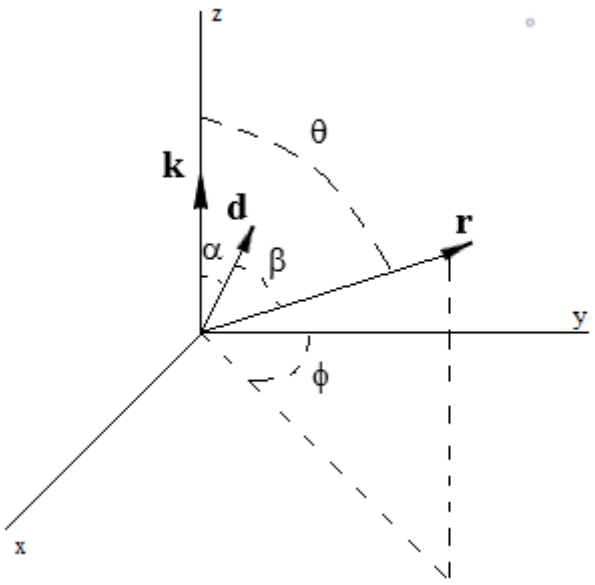

We clearly have

$$\mathbf{d} = d(\sin\alpha, \cos\alpha) \tag{B.5}$$

so that

$$\tilde{V}_{dd}(\mathbf{k}) = \int d\mathbf{r} V_{dd}(\mathbf{r}) e^{-i\mathbf{k}\cdot\mathbf{r}} \int_0^{2\pi} d\phi \int_0^{\pi} d\theta \sin\theta \int_b^{\infty} dr r^2 \frac{C_{dd}}{4\pi} \frac{1 - cos^2\beta}{r^3} e^{-ikrcos\theta} \tag{B.6}$$

where b is a small radius cut-off, introduced momentaneously to avoid any divergence. We can also write

$$\cos\beta = \frac{\mathbf{d}\cdot\mathbf{r}}{dr} = \frac{x\sin\alpha + z\cos\alpha}{r} = \sin\theta\cos\phi\sin\alpha + \cos\alpha\cos\theta \tag{B.7}$$

so that the integral over ϕ gives

$$\int_0^{2\pi} d\phi \left[1 - 3(\sin\theta\cos\phi\sin\alpha + \cos\alpha\cos\theta)^2\right] = 2\pi - 3\pi\sin^2\theta\sin^2\alpha - 6\pi\cos^2\alpha\cos^2\theta \tag{B.8}$$

We plug this expression into B.6 and integrate over θ, and fixing $x = \cos\theta$ and $u = kr$ we obtain

$$\int_0^\pi d\theta \sin\theta e^{-ikr\cos\theta}\left[2\pi - 3\pi\sin^2\theta\sin^2\alpha - 6\pi\cos^2\alpha\cos^2\theta\right] =$$
$$\int_{-1}^{1} dx e^{-iux}[2\pi - 3\pi(1-x^2)\sin^2\alpha - 6\pi\cos^2\alpha x^2]$$
$$\pi(3\cos^2\alpha - 1)\int_{-1}^{1} dx e^{-iux}(1-3x^2)$$
$$4\pi(1-3\cos^2\theta)\left[\frac{\sin u}{u} + 3\frac{\cos u}{u^2} - 3\frac{\sin u}{u^3}\right] \tag{B.9}$$

Final integration over $u = kr$ then gives

$$\tilde{V}_{dd}(\mathbf{k}) = C_{dd}(1-3\cos^2\alpha)\left[\frac{\cos(kb)}{(kb)^2} - \frac{sin(kb)}{(kb)^3}\right] \tag{B.10}$$

and taking the final limit $kb \to 0$ we obtain

$$\tilde{V}_{dd}(\mathbf{k}) = \frac{C_{dd}}{3}(3\cos^2\alpha - 1) \tag{B.11}$$

Appendix C

Calculation of the LHY correctin

We now show how the LHY correction can be computed, following [58, 32, 35].
Consider a homogeneous system of bosons described by the second quantization hamiltonian

$$\hat{H} = \sum_{\mathbf{k}} \frac{\hbar^2 k^2}{2m} \hat{a}^\dagger_{\mathbf{k}} \hat{a}_{\mathbf{k}} + \frac{1}{2V} \sum_{\mathbf{k},\mathbf{p},\mathbf{q}} V_{\mathbf{q}} \hat{a}^\dagger_{\mathbf{k}+\mathbf{q}} \hat{a}^\dagger_{\mathbf{p}-\mathbf{q}} \hat{a}_{\mathbf{p}} \hat{a}_{\mathbf{k}} \tag{C.1}$$

For a weakly interacting system, at zero temperature, we can follow Bogoliubov prescription and substitute the ground state (zero momentum) creation and destruction operators by *c-numbers*, according to

$$\hat{a}_0 \to \sqrt{N_0} \tag{C.2}$$

$$\hat{a}^\dagger_0 \to \sqrt{N_0} \tag{C.3}$$

where N_0 is the number of particles in the condensate, supposed to be macroscopic. Then, one can separate, in the hamiltonian, the various terms that contains powers of N_0 and, having supposed that it is macroscopic, keep only terms which are, at least, linear in N_0, obtaining

$$\hat{H} = \sum_{\mathbf{k}} \left(\frac{\hbar^2 k^2}{2m} + \frac{N_0 (V_0 + V_{\mathbf{k}})}{V} \right) \hat{a}^\dagger_{\mathbf{k}} \hat{a}_{\mathbf{k}} + \frac{1}{2} N_0^2 V_0 + \frac{N_0}{2V} {\sum_{\mathbf{k}}}' V_{\mathbf{k}} (\hat{a}^\dagger_{\mathbf{k}} \hat{a}^\dagger_{-\mathbf{k}} + \hat{a}_{\mathbf{k}} \hat{a}_{-\mathbf{k}}) \tag{C.4}$$

where the prime symbol means that the term with $\mathbf{k} = 0$ is excluded from the sum. In hypothesis of small depletion, we can substitute N_0 with N, the total number of bosons, in the last term, while in the second term one must be more carefull and make the appopriate substitution

$$N_0 = N - {\sum_{\mathbf{k}}}' \hat{a}^\dagger_{\mathbf{k}} \hat{a}_{\mathbf{k}} \tag{C.5}$$

obtaining finally

$$\hat{H} = \sum_{\mathbf{k}} \left(\frac{\hbar^2 k^2}{2m} + \frac{N V_{\mathbf{k}}}{V} \right) \hat{a}^\dagger_{\mathbf{k}} \hat{a}_{\mathbf{k}} + \frac{1}{2} N^2 V_0 + \frac{N}{2V} {\sum_{\mathbf{k}}}' V_{\mathbf{k}} (\hat{a}^\dagger_{\mathbf{k}} \hat{a}^\dagger_{-\mathbf{k}} + \hat{a}_{\mathbf{k}} \hat{a}_{-\mathbf{k}}) \tag{C.6}$$

This hamiltonian can be readily diagonalized through a Bogoliubov transformation, namely

$$\hat{a}_{\mathbf{k}} = u_{\mathbf{k}}\hat{\alpha}_{\mathbf{k}} - v_{\mathbf{k}}\hat{\alpha}^{\dagger}_{-\mathbf{k}} \tag{C.7}$$

where $u_{\mathbf{k}}$ and $v_{\mathbf{k}}$ satisfy

$$u^2_{\mathbf{k}} - v^2_{\mathbf{k}} = 1 \tag{C.8}$$

in order for the transformation to be canonical. The operators $\hat{\alpha}_{\mathbf{k}}$ are required to be bosonic operators, and the "quasi-particles" they act on are interpreted as elementary excitations of the condensate. The resulting hamiltonian is diagonalized by requiring

$$u_{\mathbf{k}}, v_{\mathbf{k}} = \frac{1}{2}\left[\frac{\frac{\hbar^2k^2}{2m} + \frac{NV_{\mathbf{k}}}{V}}{E_{\mathbf{k}}} \pm 1\right] \tag{C.9}$$

with

$$E_{\mathbf{k}} = \sqrt{\frac{\hbar^2k^2}{2m}\left[\frac{\hbar^2k^2}{2m} + \tilde{V}(\mathbf{k})\right]} \tag{C.10}$$

that is exactly 1.36, and finding finally

$$\hat{H} = \frac{1}{2}N^2V_0 + \frac{1}{2}{\sum_{\mathbf{k}}}'\left(E_{\mathbf{k}} - \frac{\hbar^2k^2}{2m} - \frac{NV_{\mathbf{k}}}{V}\right) + {\sum_{\mathbf{k}}}' E_{\mathbf{k}}\hat{\alpha}^{\dagger}_{\mathbf{k}}\hat{\alpha}_{\mathbf{k}} \tag{C.11}$$

The quasi-particles generated by $\hat{\alpha}_{\mathbf{k}}$ are interpreted as elementary excitations of the condensate, and so $E_{\mathbf{k}}$ is their excitation spectrum. This is clearly equal to 1.36, and its properties have been discussed previously. What is new now is that the first two terms of C.11 represents, respectively, the mean field ground state energy of the homogeneous system of bosons, and the first order quantum correction. Thus, we find that the first order quantum correction to the mean field ground state energy is given by

$$\Delta E = \frac{1}{2}{\sum_{\mathbf{k}}}'\left(E_{\mathbf{k}} - \frac{\hbar^2k^2}{2m} - nV_{\mathbf{k}}\right) \tag{C.12}$$

where n is the density of the system. To evaluate the correction C.12, one needs a good model for the interaction potential $V_{\mathbf{k}}$. Once again, because of the fact that this result is valid only for weak coupling, one cannot use the real interatomic potential, because it is very strongly repulsive at short distances. Thus, we need to use the previously discussed pseudo-potentials 1.25 or 1.27. In both cases, however, the correction diverges, which is due to the fact that perturbation theory does not describe properly the problem. To regularize this divergence, one can consider the second order expansion of the scattering length in the interaction potential, which reads [58, 35]

$$\frac{4\pi a\hbar^2}{m} = V_0 - \frac{m}{\hbar^2}\int \frac{d\mathbf{q}}{(2\pi)^3}\frac{V(\mathbf{q})V(-\mathbf{q})}{q^2} \tag{C.13}$$

or

$$V_0 = \frac{4\pi a\hbar^2}{m} + \frac{m}{\hbar^2}\int \frac{d\mathbf{q}}{(2\pi)^3}\frac{V(\mathbf{q})V(-\mathbf{q})}{q^2} \tag{C.14}$$

Plugging this into C.12 and evaluating the sum as an integral, we find, for the case of only short-range potentials

$$\frac{E_0}{V} = \frac{1}{2}gn^2\left[1 + \frac{128}{15\sqrt{\pi}}\sqrt{na^3}\right] \tag{C.15}$$

that is the classical LHY result, while for the dipolar case, with the pseudo-potential given by 1.27, we find

$$\frac{E_0}{V} = \frac{1}{2}gn^2\left[1 + \frac{128}{15\sqrt{\pi}}\sqrt{na^3}F(\epsilon_{dd})\right] \tag{C.16}$$

with

$$F(\epsilon_{dd}) = \frac{1}{2}\int_0^\pi d\theta sin\theta[1 + \epsilon_{dd}(3cos^2\theta - 1)]^{\frac{5}{2}} \tag{C.17}$$

This approach is valid only in the limit of small depletion. The condensate depletion in presence of quantum fluctuations can be estimated as

$$\frac{N - N_0}{N} = \frac{1}{N}\langle 0|\sum_{\mathbf{k}}{}' \hat{a}^\dagger_{\mathbf{k}}\hat{a}_{\mathbf{k}}|0\rangle \tag{C.18}$$

where $|0\rangle$ is the vacuum of the quasi-particle operators $\hat{\alpha}_{\mathbf{k}}$, that is the condensate. Thus, we find

$$\frac{N - N_0}{N} = \frac{1}{N}\langle 0|\sum_{\mathbf{k}}{}' v^2_{\mathbf{k}}|0\rangle \tag{C.19}$$

or, using the form of v_k previously calculated and tranforming the sum into an integral, we find, for purely contact interaction,

$$\frac{N - N_0}{N} = \frac{8}{3\sqrt{\pi}}\sqrt{na^3} \tag{C.20}$$

or, for the case of contact plus dipolar interaction

$$\frac{N - N_0}{N} = \frac{8}{3\sqrt{\pi}}\sqrt{na^3}F_D(\epsilon_{dd}) \tag{C.21}$$

with

$$F_D(\epsilon_{dd}) = \frac{1}{2}\int_0^\pi d\theta sin\theta\left(1 - \epsilon_{dd}(3cos^2\theta - 1)\right)^{\frac{3}{2}} \tag{C.22}$$

The condensate depletion C.21 must be small in order for this theory to be valid. Thus, in all the simulations performed in this thesis, it is always kept to be of order 10^{-3} or smaller.

Appendix D

Alternative derivation of the NLGPE

In chapter 2, the NLGPE used to calculate the ground state of the system has been derived using a variational approach. However, as mentioned, in literature the equation is usually derived from a more rigorous approach based on second quantization. In particular, following [32, 35] we can start with a hamiltonian written in second quantization as

$$\begin{aligned}\hat{H} = &\int d\mathbf{r}\hat{\Phi}^\dagger(\mathbf{r})\left(-\frac{\hbar^2\nabla^2}{2m} + V_{ext}(\mathbf{r})\right)\hat{\Phi}(\mathbf{r}) \\ &+ \frac{1}{2}\int d\mathbf{r}d\mathbf{r}'\hat{\Phi}^\dagger(\mathbf{r})\hat{\Phi}^\dagger(\mathbf{r}')V(\mathbf{r}-\mathbf{r}')\hat{\Phi}(\mathbf{r}')\hat{\Phi}(\mathbf{r})\end{aligned} \tag{D.1}$$

where $\hat{\Phi}^\dagger(\mathbf{r})$ and $\hat{\Phi}(\mathbf{r})$ are bosonic creation and destruction fields, satisfying the usual bosonic commutation relations

$$\begin{aligned}\left[\hat{\Phi}(\mathbf{r}), \hat{\Phi}^\dagger(\mathbf{r}')\right] &= \delta(\mathbf{r}-\mathbf{r}') \\ \left[\hat{\Phi}(\mathbf{r}), \hat{\Phi}(\mathbf{r}')\right] &= \left[\hat{\Phi}^\dagger(\mathbf{r}), \hat{\Phi}^\dagger(\mathbf{r}')\right] = 0\end{aligned} \tag{D.2}$$

and $V(\mathbf{r}-\mathbf{r}')$ is the two-body interatomic potential. The field $\hat{\Phi}$ evolve in time according to the Heisenberg equation of motion

$$\begin{aligned}i\hbar\frac{\partial}{\partial t}\hat{\Phi}(\mathbf{r}) &= \left[\hat{\Phi}(\mathbf{r}), \hat{H}\right] \\ &= -\left(\frac{\hbar^2\nabla^2}{2m} + V_{ext}(\mathbf{r}) + \int d\mathbf{r}'\hat{\Phi}^\dagger(\mathbf{r}')V(\mathbf{r}-\mathbf{r}')\hat{\Phi}(\mathbf{r}')\right)\hat{\Phi}(\mathbf{r})\end{aligned} \tag{D.3}$$

In the case of small depletion, that is in conditions in which the number of particles in the condensate is macroscopic, we can use Bogoliubov prescription and substitute the microscopic quantum field $\hat{\Phi}$ with a macroscopic classical field Φ. At the same time,

we can substitute the real interatomic potential with the proper pseudopotential 1.25 or 1.27, obtaining respectively the time dependent version of the GPE 1.26 and the NLGPE 1.28.

Bibliography

[1] P. Kapitza. Viscosity of liquid helium below the λ-point. *Nature*, 141:74 EP –, Jan 1938.

[2] J. F. ALLEN and A. D. MISENER. Flow of liquid helium ii. *Nature*, 141:75 EP –, Jan 1938.

[3] F. London. The λ-phenomenon of liquid helium and the bose-einstein degeneracy. *Nature*, 141:643 EP –, Apr 1938.

[4] L. Tisza. Transport phenomena in helium ii. *Nature*, 141:913 EP –, May 1938.

[5] L. Landau. Theory of the superfluidity of helium ii. *Phys. Rev.*, 60:356–358, Aug 1941.

[6] N. N. Bogolyubov. On the theory of superfluidity. *J. Phys.(USSR)*, 11:23–32, 1947. [Izv. Akad. Nauk Ser. Fiz.11,77(1947)].

[7] M. H. Anderson, J. R. Ensher, M. R. Matthews, C. E. Wieman, and E. A. Cornell. Observation of bose-einstein condensation in a dilute atomic vapor. *Science*, 269(5221):198–201, 1995.

[8] K. B. Davis, M. O. Mewes, M. R. Andrews, N. J. van Druten, D. S. Durfee, D. M. Kurn, and W. Ketterle. Bose-einstein condensation in a gas of sodium atoms. *Phys. Rev. Lett.*, 75:3969–3973, Nov 1995.

[9] Cheng Chin, Rudolf Grimm, Paul Julienne, and Eite Tiesinga. Feshbach resonances in ultracold gases. *Rev. Mod. Phys.*, 82:1225–1286, Apr 2010.

[10] Axel Griesmaier, Jörg Werner, Sven Hensler, Jürgen Stuhler, and Tilman Pfau. Bose-einstein condensation of chromium. *Phys. Rev. Lett.*, 94:160401, Apr 2005.

[11] Mingwu Lu, Nathaniel Q. Burdick, Seo Ho Youn, and Benjamin L. Lev. Strongly dipolar bose-einstein condensate of dysprosium. *Phys. Rev. Lett.*, 107:190401, Oct 2011.

[12] K. Aikawa, A. Frisch, M. Mark, S. Baier, A. Rietzler, R. Grimm, and F. Ferlaino. Bose-einstein condensation of erbium. *Phys. Rev. Lett.*, 108:210401, May 2012.

[13] T. Koch, T. Lahaye, J. Metz, B. Fröhlich, A. Griesmaier, and T. Pfau. Stabilization of a purely dipolar quantum gas against collapse. *Nature Physics*, 4:218 EP –, Feb 2008.

[14] Holger Kadau, Matthias Schmitt, Matthias Wenzel, Clarissa Wink, Thomas Maier, Igor Ferrier-Barbut, and Tilman Pfau. Observing the rosensweig instability of a quantum ferrofluid. *Nature*, 530:194 EP –, Feb 2016.

[15] Igor Ferrier-Barbut, Matthias Wenzel, Matthias Schmitt, Fabian Böttcher, and Tilman Pfau. Onset of a modulational instability in trapped dipolar bose-einstein condensates. *Phys. Rev. A*, 97:011604, Jan 2018.

[16] Matthias Schmitt, Matthias Wenzel, Fabian BÃ¶ttcher, Igor Ferrier-Barbut, and Tilman Pfau. Self-bound droplets of a dilute magnetic quantum liquid. *Nature*, 539:259 EP –, Nov 2016.

[17] F. Wächtler and L. Santos. Quantum filaments in dipolar bose-einstein condensates. *Phys. Rev. A*, 93:061603, Jun 2016.

[18] D. Baillie, R. M. Wilson, R. N. Bisset, and P. B. Blakie. Self-bound dipolar droplet: A localized matter wave in free space. *Phys. Rev. A*, 94:021602, Aug 2016.

[19] L. Chomaz, R. M. W. van Bijnen, D. Petter, G. Faraoni, S. Baier, J. H. Becher, M. J. Mark, F. Wächtler, L. Santos, and F. Ferlaino. Observation of roton mode population in a dipolar quantum gas. *Nature Physics*, 14(5 .):442–446, 2018.

[20] T Lahaye, C Menotti, L Santos, M Lewenstein, and T Pfau. The physics of dipolar bosonic quantum gases. *Reports on Progress in Physics*, 72(12):126401, 2009.

[21] Bryce Gadway and Bo Yan. Strongly interacting ultracold polar molecules. *Journal of Physics B: Atomic, Molecular and Optical Physics*, 49(15):152002, 2016.

[22] T. Lahaye, J. Metz, B. Fröhlich, T. Koch, M. Meister, A. Griesmaier, T. Pfau, H. Saito, Y. Kawaguchi, and M. Ueda. *d*-wave collapse and explosion of a dipolar bose-einstein condensate. *Phys. Rev. Lett.*, 101:080401, Aug 2008.

[23] Elizabeth A. Donley, Neil R. Claussen, Simon L. Cornish, Jacob L. Roberts, Eric A. Cornell, and Carl E. Wieman. Dynamics of collapsing and exploding bose-einstein condensates. *Nature*, 412:295 EP –, Jul 2001. Article.

[24] C. A. Sackett, J. M. Gerton, M. Welling, and R. G. Hulet. Measurements of collective collapse in a bose-einstein condensate with attractive interactions. *Phys. Rev. Lett.*, 82:876–879, Feb 1999.

[25] P. Hohenberg and W. Kohn. Inhomogeneous electron gas. *Phys. Rev.*, 136:B864–B871, Nov 1964.

[26] L. Salasnich. *Quantum Physics of Light and Matter*. Springer, 2014.

[27] W. Kohn and L.J. Sham. Self-consistent equations including exchange and correlation effects. *Phys. Rev.*, 140, Nov 1965.

[28] D.R. Hartree. The wave mechanics of an atom with a non-coulomb central field. part i. theory and methods. *Proc. Cambridge Philos. Soc.*, 24, 1928.

[29] D.O. Jones and O. Gunnarsson. The density functional formalism, its applications and prospects. *Reviews of Modern Physics*, 61, july 1989.

[30] Landau Lev D. and Evgenij Lifsic. *Quantum mechanics: non-relativistic theory.* Butterworth-Heinemann, 2010.

[31] Kerson Huang and C. N. Yang. Quantum-mechanical many-body problem with hard-sphere interaction. *Phys. Rev.*, 105:767–775, Feb 1957.

[32] L.P. Pítajevskíj and S. Stringari. *Bose-Einstein Condensation.* International Series of Monographs on Physics. Clarendon Press, 2003.

[33] S. Yi and L. You. Trapped condensates of atoms with dipole interactions. *Phys. Rev. A*, 63:053607, Apr 2001.

[34] M. Marinescu and L. You. Controlling atom-atom interaction at ultralow temperatures by dc electric fields. *Phys. Rev. Lett.*, 81:4596–4599, Nov 1998.

[35] Aristeu R. P. Lima and Axel Pelster. Quantum fluctuations in dipolar bose gases. *Phys. Rev. A*, 84:041604, Oct 2011.

[36] Igor Ferrier-Barbut, Holger Kadau, Matthias Schmitt, Matthias Wenzel, and Tilman Pfau. Observation of quantum droplets in a strongly dipolar bose gas. *Phys. Rev. Lett.*, 116:215301, May 2016.

[37] D. S. Petrov. Quantum mechanical stabilization of a collapsing bose-bose mixture. *Phys. Rev. Lett.*, 115:155302, Oct 2015.

[38] D. G. Henshaw and A. D. B. Woods. Modes of atomic motions in liquid helium by inelastic scattering of neutrons. *Phys. Rev.*, 121:1266–1274, Mar 1961.

[39] F. Cinti, P. Jain, M. Boninsegni, A. Micheli, P. Zoller, and G. Pupillo. Supersolid droplet crystal in a dipole-blockaded gas. *Phys. Rev. Lett.*, 105:135301, Sep 2010.

[40] Massimo Boninsegni and Nikolay V. Prokof'ev. Colloquium: Supersolids: What and where are they? *Rev. Mod. Phys.*, 84:759–776, May 2012.

[41] Oliver Penrose and Lars Onsager. Bose-einstein condensation and liquid helium. *Phys. Rev.*, 104:576–584, Nov 1956.

[42] Eugene P. Gross. Unified theory of interacting bosons. *Phys. Rev.*, 106:161–162, Apr 1957.

[43] C. N. Yang. Concept of off-diagonal long-range order and the quantum phases of liquid he and of superconductors. *Rev. Mod. Phys.*, 34:694–704, Oct 1962.

[44] A. J. Leggett. Can a solid be "superfluid"? *Phys. Rev. Lett.*, 25:1543–1546, Nov 1970.

[45] E. Kim and M. H. W. Chan. Probable observation of a supersolid helium phase. *Nature*, 427:225 EP –, Jan 2004.

[46] Duk Y. Kim and Moses H. W. Chan. Absence of supersolidity in solid helium in porous vycor glass. *Phys. Rev. Lett.*, 109:155301, Oct 2012.

[47] Francesco Ancilotto, Maurizio Rossi, and Flavio Toigo. Supersolid structure and excitation spectrum of soft-core bosons in three dimensions. *Phys. Rev. A*, 88:033618, Sep 2013.

[48] T. Macrì, F. Maucher, F. Cinti, and T. Pohl. Elementary excitations of ultracold soft-core bosons across the superfluid-supersolid phase transition. *Phys. Rev. A*, 87:061602, Jun 2013.

[49] N. Seplveda, C. Josserand, and S. Rica. Superfluid density in a two-dimensional model of supersolid. *The European Physical Journal B*, 78(4):439447, 2010.

[50] J. Goldstone. Field theories with superconductor solutions. *J. Nuovo cim*, 19, 1961.

[51] Anthony J. Leggett. *Quantum liquids: Bose condensation and Cooper pairing in condensed-matter systems*. Oxford Univ. Press, 2015.

[52] W. Ketterle, D. S. Durfee, and D. M. Stamper-Kurn. Making, probing and understanding bose-einstein condensates, 1999.

[53] Hiroki Saito. Path-integral monte carlo study on a droplet of a dipolar boseeinstein condensate stabilized by quantum fluctuation. *Journal of the Physical Society of Japan*, 85(5):053001, 2016.

[54] Shai Ronen, Daniele C. E. Bortolotti, and John L. Bohn. Radial and angular rotons in trapped dipolar gases. *Phys. Rev. Lett.*, 98:030406, Jan 2007.

[55] D. Baillie, R. M. Wilson, and P. B. Blakie. Collective excitations of self-bound droplets of a dipolar quantum fluid. *Phys. Rev. Lett.*, 119:255302, Dec 2017.

[56] S. Giovanazzi and D. H. J. O'dell. Instabilities and the roton spectrum of a quasi-1d bose-einstein condensed gas with dipole-dipole interactions. *The European Physical Journal D*, 31(2):439445, 2004.

[57] Eric W. Weisstein. Convolution theorem. `http://mathworld.wolfram.com/ConvolutionTheorem.html`.

[58] Alexander L. Fetter and John Dirk Walecka. *Quantum theory of many-particle systems*. Dover Publications, 2003.